



Resilience of wave energy farms using metocean dependent failure rates and repair operations

Malin Götteman^{a,b,*}, Zahra Shahroozi^a, Charitini Stavropoulou^a, Eirini Katsidoniotaki^{a,b}, Jens Engström^a

^a Uppsala University, Department of Electrical Engineering, The Ångström Lab, Uppsala, 752 37, Sweden

^b Centre of Natural Hazards and Disaster Science (CNDS), Villavägen 16, Uppsala, 752 36, Sweden

ARTICLE INFO

Keywords:
Wave energy
Farms
Resilience
Failure rates

ABSTRACT

Emerging offshore renewable energy technologies are expected to become an important part of the future energy system, and reliability for these new technologies in different metocean scenarios must be guaranteed. This poses a challenge in extreme weather scenarios like storms, in particular for less mature technologies such as wave energy. Not only the offshore survivability must be controlled; the restoration after disruptive events and failures should be addressed and optimized. Offshore operations are costly and cannot be carried out if the weather is too harsh, and the resulting downtime after failures may be financially devastating for projects. In this paper, the resilience of large wave energy systems is studied with respect to wave conditions, metocean dependent failure rates, and weather windows available for offshore repair operations. A metocean- and time-dependent failure rate is derived based on a Weibull distribution, which is a novelty of the paper. The performance of the farm is assessed using the varying failure rates and metocean data at different offshore sites. Critical metocean thresholds for different offshore vessels are considered, and the resilience is quantified using relevant measures such as unavailability and expected energy not supplied. The resilience analysis is coupled to an economic assessment of the wave farm and different repair strategies. Our results show that the commonly used assumption of constant failure rates is seen to overestimate the annual energy production than when a more realistic varying failure rate is used. Two offshore sites are compared, and the availability is found to be higher at the calmer site. Most of the evaluated repair strategies cannot be considered to be economically justified, when compared to the cost of the energy not supplied.

1. Introduction

To exploit the vast amounts of renewable energy available offshore, renewable energy systems (RES) are today being installed around the world at a rapid speed. At the US Pacific coast alone, the available offshore wind, wave and tidal energy potential is estimated sufficient to supply energy to a million households (Schwartz et al., 2010; Haas et al., 2011; Jacobson et al., 2011). The majority of the installations are offshore wind turbines installed in shallow waters, but investments are also being put into less mature energy technologies such as wave and tidal energy. Wave energy is a promising energy source, but no concept has yet demonstrated a performance and cost compatible with offshore wind (Chang et al., 2018), although several technologies are currently in the pre-commercial testing phase.

The electric grid is a cornerstone of modern society. Disruption in the electricity supply would have a considerable impact on the

society, and the increasing penetration of offshore RES in the electric grid implies that the reliability of these new energy systems must be targeted and guaranteed. For less mature offshore RES such as floating offshore wind, wave and tidal energy, this still poses a knowledge gap, and in particular the vulnerability to, or the survivability in, weather extremes is a challenge. This vulnerability not only affects the reliability of the electricity supply, but also to a large extent the costs of the system, as offshore operations are extremely costly (Clark and DuPont, 2018).

Vulnerability has been identified as one of the main challenges for offshore wind systems (Carroll et al., 2016; Gintautas and Sørensen, 2017), and the challenge can be expected to be even larger in wave and tidal energy, due to the low maturity and large diversity in the developed technologies. In addition, wave energy systems are often designed to be highly dynamical and responsive, which poses an additional challenge to the reliability, at least at the current stage of

* Corresponding author at: Uppsala University, Department of Electrical Engineering, The Ångström Lab, Uppsala, 752 37, Sweden.

E-mail addresses: malin.goteman@angstrom.uu.se (M. Götteman), zahra.shahroozi@angstrom.uu.se (Z. Shahroozi), charitini.stavropoulou@angstrom.uu.se (C. Stavropoulou), eirini.katsidoniotaki@angstrom.uu.se (E. Katsidoniotaki), jens.engstrom@angstrom.uu.se (J. Engström).

<https://doi.org/10.1016/j.oceaneng.2023.114678>

Received 8 February 2022; Received in revised form 13 April 2023; Accepted 24 April 2023

Available online 5 May 2023

0029-8018/© 2023 The Author(s). Published by Elsevier Ltd. This is an open access article under the CC BY license (<http://creativecommons.org/licenses/by/4.0/>).

technology development. Indeed, Walker et al. (2011), O'Connor et al. (2013a) and Clark and DuPont (2018) all concluded that failures and the related downtime is one of the main costs for wave energy systems. The offshore site can only be accessed during periods of calm metocean parameters, during so called open *weather windows*.

Resilience of a system, defined as the “ability to anticipate, absorb, respond, and rapidly recover from an external, high-impact, low-probability disturbance” (Panteli and Mancarella, 2015), includes not only low vulnerability to different hazards, but also the recovery process when failures have occurred. Both downtime and offshore repair operations may become very costly, and to obtain offshore energy systems with a low levelized cost of energy (LCOE), the recovery process after failures must be analysed when optimizing the system. Another term often used when quantifying the reliability of an energy system is *availability*, defined as the percentage of the time that the system is able to operate and produce power according to its design specifications. Availability and performance as functions of weather windows have been studied within the context of wave energy in a range of works. Aizpurua et al. (2022), developed a method for conditional anomaly detection for air turbines in the Mutriku wave power plant, using rare real data as input. O'Connor et al. (2012, 2013b) studied weather-dependent availability and accessibility of offshore RES. The results suggested that the accessibility at some sites on the Irish west coast was too low to allow for offshore maintenance, and that failed devices at these sites should always be transported to shore for repair. Procedures for assessing accessibility of marine energy sites were evaluated by Noguera et al. (2010), and the time-series approach was recommended over the simpler stochastic method. de Andrés et al. (2015) compared failures of wave energy converters (WECs) as well as operation and maintenance (O&M) operations for different sites, and it was concluded that failures that need a long weather window to repair are demanding because they increase the overall downtime, despite their rate of occurrence being low. Availability and performance of a farm of 5 Pelamis WECs was studied by Rinaldi et al. (2016a,b), and it was seen that the results depended heavily on the choice of vessels and their metocean thresholds for operation. The availability of a 10 MW wave energy farm was studied by Kennedy et al. (2017), and it was seen that the combined impact of weather window criteria, reliability levels and available vessels can cause a backlog of failures that cannot be rectified, which would force the availability of the farm to an unacceptable level. Götteman et al. (2018) used different input values of failure rates, repair rates, and metocean thresholds to study the availability of a wave farm, and it was seen that a farm installed at a site with milder wave climate could potentially achieve a higher annual energy production than if it was installed at a site with a more energetic wave climate, due to the lower availability at the latter site. Walker et al. (2011, 2013) studied the cost implications of maintenance operations, and it was seen that the downtime due to weather windows has a large impact on the total costs. Accessible periods for installation were identified, using the UK WaveHub site as a test case. Motivated by the lower accessibility of offshore RES as compared to onshore systems, the approach of continuous condition-based maintenance strategies was reviewed by Mérigaud and Ringwood (2016), particularly highlighting the expertise that can be drawn from the more mature offshore wind sector and other established offshore technologies, where risk-based inspection and maintenance planning are standard procedures. A framework for assessing reliability, availability, and maintainability was presented by Rinaldi et al. (2018), where failures were modelled based on adjusted failure rates from components obtained from Thies et al. (2009). The models for the failures, accessibility, O&M, and energy absorption by the farm were combined in a Monte-Carlo simulation to obtain probabilistic results for the performance of a Spar Buoy wave farm over 10 years. One of the conclusions of the study was that repair costs are the major driver of O&M costs, and that the failures of a few components might make the difference between a successful and unsuccessful project. Guanche et al.

(2015) computed O&M costs at different sites with different accessibility. 60 years reanalysis data was used, and the accessibility was studied for different vessel thresholds. The authors concluded that O&M costs were considerably lower in milder wave climates, and recommended milder locations when testing prototypes and non-mature technologies.

In the research area of the electric grid, resilience is a well-known concept and analysis measure (Bie et al., 2017). Kiel and Kjølle (2019) studied the power system availability as a function of weather exposure. Instead of using constant average failure rates, time dependent failure rates were used, and this was seen to affect the resilience of the system to a large extent, as measured in energy not supplied (ENS).

The resilience concept has been applied for offshore wind systems (Wang et al., 2019; Feng et al., 2019), but it has not been studied within the context of wave energy systems to the same degree. As defined above, resilience deals not only with the vulnerability to hazards, but also with the recovery process. Even if vulnerability of wave energy systems to extreme wave conditions is a well-studied research area both numerically and experimentally (Zhao and Hu, 2012; Ransley, 2015; Hann et al., 2015; Götteman et al., 2015a; Rafiee and Fiévez, 2015; Madhi and Yeung, 2018), very few have connected the extreme wave loads impacted on the system to the probability of failure, and even fewer to restoration and performance during and after disruptions. One of the few papers that have discussed wave energy systems in the framework of resilience is by Korde (2019), motivated by the hypothesis that wave energy could provide a more resilient energy system to remote and isolated electric grids. However, the vulnerability of the wave energy system to extreme events was not studied explicitly by Korde (2019) (rather, it was assumed to be low); instead the resilience was studied as a method to recover full power capacity by control optimization.

As reviewed above, the availability of wave energy systems as function of metocean conditions, failures and offshore vessels has been assessed in a number of works (O'Connor et al., 2012, 2013a,b; Walker et al., 2013; de Andrés et al., 2015; Guanche et al., 2015; Rinaldi et al., 2016a,b; Kennedy et al., 2017; Götteman et al., 2018; Clark and DuPont, 2018). However, despite the expectation that the probability of failures depends on the environmental loads (e.g., Guanche et al., 2015) concluded that failures should be more frequent during winter time due to the harsher weather, and larger peak loads have been measured or modelled during extreme wave scenarios in a large number of works), this has, to the best of knowledge of the authors, not been taken into account in previous works. In wind energy, as well as in other engineering areas, the use of a fragility curve is a common strategy to determine the vulnerability of the system due to external environmental loads.

In this paper, we take the similar approach to wave energy systems. The metocean dependent vulnerability of the system is then used to derive a failure rate that is metocean dependent and changing over the year due to the wave loads. This gives a more realistic prediction of the failures, as they are more likely to happen during storms and violent metocean conditions. As recommended by Noguera et al. (2010) and inspired by the power system resilience analysis by Kiel and Kjølle (2019), a time-domain analysis of the availability of the system is carried out.

Due to the lack of published data for wave energy systems, very little is known about the actual offshore performance, both relating to the power production and to the failure in different conditions. The approach of the current paper is to develop a methodology of assessing the availability and resilience of wave energy systems due to weather conditions, by using the data that is available, and constructing the other required input values based on experience, modelling, and on data for related systems. To analyse the performance of the wave energy farm given the number of available devices and sea state at each time step, a simplified model for the park interaction is applied.

The novelties of the paper are that (1) failures of a wave energy system are connected to the environmental loads; (2) weather data for

offshore sites is analysed, both to predict long-term extreme weather predictions, and for detailed time-domain studies, to which the varying failure rates are connected; (3) a new simplified model is applied for the park interaction, which allows a performance evaluation of the total power production without a time-consuming simulation of the hydrodynamic interactions in the farm; (4) the availability and resilience of a large wave energy farm is derived as functions of the weather dependent failure rates and the different offshore vessels, and quantified in terms of appropriate measures; (5) an economical assessment is carried out, both of the net present value as function of the power ratings of the WECs, and of the different repair vessels and their operational weather thresholds.

The rest of the paper is structured as follows. The theory and method are presented in Section 2, including extreme weather analysis, weather dependent failure rates, and the resulting power production by the farm. Results are then presented in Section 3. In Section 4, uncertainties related to the method and the input parameters are discussed, and strategies for future work are outlined. Finally, conclusions are presented in Section 5.

2. Theory and method

The aim of this paper is to study the performance and resilience of an offshore wave energy farm as a function of weather conditions. The performance and resilience will be analysed quantitatively in terms of power production (or the lack thereof), availability, and economical metrics. For this matter, we must first *characterize the weather parameters* and *model the wave energy system*. Then, an understanding of the *probability of failures in different weather scenarios* must be developed, as well as a realistic modelling of *conditions during which the devices can be repaired* after they have failed. Finally, assembling this information gives input to the *system availability and the power production* as a function of the extreme weather conditions. In the next five subsections, theory and methods for these tasks will now be reviewed and developed.

2.1. Extreme weather characterization

The low-probability, high impact events of interest when assessing the resilience of offshore RES are extreme weather conditions, such as high winds and waves occurring during storms. To understand the probability of failure due to an external hazard, the probability of the hazard must be understood. Here, we will describe the extreme value theory used to analyse the weather hazard, and provide details for the offshore sites and weather data used in the paper.

2.1.1. Extreme value theory

Two common methods to analyse extreme value data are the peak-over-threshold method and the block-maxima method. In the peak-over-threshold method, all data points above a specified threshold are identified as the extreme value points, and in the block-maxima method, the data is divided into non-overlapping periods (blocks) of equal and suitable size, and the maximum is identified in each block. Both methods come with their advantages and drawbacks; in the peak-over-threshold method, the results are sensitive to the choice of threshold, and in the block maxima method some extremes may be missed since only the maximum in each block is captured. In the block maxima method, the periods should be long enough to cover seasonal periodicities, and long-term (over decades) data is required. Due to the availability of long-term data in this project, block size can be chosen to one year, and the block-maxima method will be applied to avoid the bias of thresholds.

Let $(\bar{x}_{11}, \dots, \bar{x}_{m1}, \bar{x}_{21}, \dots, \bar{x}_{mn})$ be an observation that can be split into n blocks, each of size m , for instance the recorded significant wave height or average wind speed each hour m during n years. Let $x_j = \max(\bar{x}_{ij})$ be the maximum values in each block. By the extreme value

theorem (Fisher and Tippett, 1928; Gnedenko, 1943), the generalized extreme value (GEV) distribution is the only possible limit distribution of properly normalized maxima of a sequence of independent and identically distributed random variables. The GEV distribution takes the form

$$f(x) = \frac{1}{\sigma} \left(1 + k \left(\frac{x - \mu}{\sigma} \right) \right)^{-(1+1/k)} e^{-\left[1 + k \left(\frac{x - \mu}{\sigma} \right) \right]^{-1/k}} \quad (1)$$

where $k \neq 0$ is the shape parameter, σ the scale parameter, and μ the location parameter. For $k > 0$, the distribution is called a GEV distribution of type II, or a Frechet distribution, whereas for $k < 0$, it is called a GEV distribution of type III, or a Weibull distribution. In the special case when $k = 0$, the distribution is said to be of type I, or a Gumbel distribution, and takes the form

$$f(x) = \frac{1}{\sigma} e^{\left(-e^{-\frac{x-\mu}{\sigma}} + \frac{x-\mu}{\sigma} \right)}. \quad (2)$$

The cumulative distribution function (CDF) of a random variable X for a probability distribution $f(x)$ is the integral

$$F_X(x) = \int_{-\infty}^x f(x') dx' \quad (3)$$

and satisfies $F_X(x) \rightarrow 0$ as $x \rightarrow -\infty$ and $F_X(x) \rightarrow 1$ as $x \rightarrow \infty$, i.e., the cumulative probability that the variable X takes *no* value or *any* finite value is zero and one, respectively. When the variable X represents a weather parameter as in this paper, $X \geq 0$ and the integral in Eq. (3) is taken from 0 to X . In the case when the probability distribution function takes the form of a GEV distribution of type II or III as in Eq. (1), the explicit form of the CDF is

$$F_X(x) = e^{-\left[1 + k \frac{x-\mu}{\sigma} \right]^{-1/k}}. \quad (4)$$

The cumulative distribution function $F_X(x)$ thus gives the probability that the variable X takes the value $X \leq x$, and conversely, the function $1 - F_X(x)$ gives the probability that the variable exceeds the value x . For instance, if X denotes the wave height and $1 - F_X(10) = 0.1$, the probability of a wave height above 10 m is 0.1; in one year, $X > 10$ m is expected to occur 0.1 times, or one time in 10 years. This defines the return period T_R as the estimated average time between $X > x$ as

$$T_R(X > x) = \frac{1}{1 - F_X(x)}, \quad (5)$$

from which follows that $F_X = 1 - 1/T_R$. Design codes for offshore structures typically stipulate that they should be able to withstand environmental loadings corresponding to return period of 100 years, or in some cases as high as 10 000 years. The choice of return period for the design codes is based on the structure and on its required degree of reliability, e.g., manned oil and gas rigs are subject to higher reliability requirements than unmanned wind turbines. For offshore RES, the recommended design return period is usually 50–100 years (IEC International Electrotechnical Commission, 2015; Coe et al., 2018).

In the same way as we can map an extreme value $X > x$ to a return period $T_R(X > x)$ by the CDF in Eq. (5), we can map the extreme value corresponding to a return period by the inverse cumulative distribution function F_X^{-1} as

$$X = F_X^{-1} \left(1 - \frac{1}{T_R} \right). \quad (6)$$

An explicit expression for the return value can also be found using the explicit expression for the cumulative distribution function in Eq. (4) and setting it equal to $1 - 1/T_R$ according to Eq. (5). Taking the logarithm of both sides and solving for x gives an equivalent explicit expression for the extreme value corresponding to return period T_R ,

$$X = \mu + \frac{\sigma}{k} \left(-1 + \left[-\ln(1 - 1/T_R) \right]^{-k} \right). \quad (7)$$

Table 1

Offshore sites considered in the study. Short name of the site used in the paper, owner, station number, location, position, period of data sample, and data parameters.

Short name	Data owner	Station	Location	Position	Period	Parameters
SE site	SMHI	35056	Almagrundet, Sweden	59.1495N 19.1297E	1976–2010	W_s, H_s, T_{avg}
US site	NDBC	44025	Long Island, NY, USA	40.251N 73.164W	1991–2020	W_s, H_s, T_{peak}

2.1.2. Sites

Two offshore sites have been studied and compared in this paper; one in the Baltic Sea close to Stockholm, Sweden, and one in the Atlantic Ocean just outside Long Island in the USA. Whereas the first site represents a very calm offshore site, the second has more energetic weather conditions. However, both represent mild wave climates, with average energy flux of 3.1 kW/m and 7.9 kW/m, respectively. Both sites are close enough to the shore and have a water depth suitable for offshore renewable energy installations. The details of the two sites are listed in Table 1. At the US site, the weather data has been recorded by the National Data Buoy Centre (NDBC) at the station numbered 44025. At the Swedish site, the wave data has been recorded by the Swedish Meteorological and Hydrological Institute (SMHI) at station 35056, and the wind data at station 99090 which has a slightly different location (59.1547N, 19.1298E). For brevity, the Swedish and US site will simply be referred to as the *SE site* and *US site*, respectively.

The wave data at the SE site has been sampled during a shorter time than the wind (1978–2003). At both sites, the average wind speed W_s and significant wave height H_s have been sampled. At the SE site, the average wave period T_{avg} during each hour has been sampled, whereas at the US site, instead the peak wave period T_{peak} has been reported.

At both sites, there are several longer and shorter periods of missing and erroneous data. This has not been considered when identifying the annual maximum for wind speed and wave height to characterize the extreme weather. When studying the hourly weather data to analyse weather windows and varying failure rates, two years of good quality data has been chosen from the respective sites. The chosen years are 1984 and 1996 for the SE and US sites, respectively.

2.2. Wave energy farms and energy absorption

2.2.1. Farm model

A wave energy converter (WEC) is a device designed to absorb the energy available in ocean waves and convert it to a useful form of energy, usually electricity. Many different wave energy concepts exist, and differ fundamentally in their dimensions, dynamics, and energy absorption technology. In this paper, we focus on generic WECs of small dimensions in relation to the wave length, so called point-absorbers.

Consider a farm of N available point-absorber WECs at time t . We will assume that the WECs are characterized by a device width D and a capture width ratio (CWR) τ , specifying how large ratio of the incident available wave energy that the device can absorb,

$$\tau = \frac{P_{abs}}{P_{avail}}. \quad (8)$$

The available power $P_{avail} = DJ$ to the WEC is obtained from the energy flux J in the waves and the device width D , and the absorbed power P_{abs} is modelled for all sea states. The numerical model is based on linear potential flow theory and solves the dynamics and power absorption of a WEC subject to incident waves. It is implemented in MATLAB and has previously been utilized and compared to experimental data for a range of different settings (Eriksson et al., 2007; Sjökvist et al., 2017).

The area of the wave farm site is of the size $L_{park} \times L_{park}$, where L_{park} is the side of the square. At each instant, instead of considering the actual positions of the WECs, we will assume that the WECs are positioned on a quadratic grid. This assumption is illustrated in Fig. 1, where instead of the actual farm in (a) we model the approximate farm layout in (b). This farm layout strategy is indeed an approximation, that could be expected to work reasonably well for large and densely populated farms subjected to realistic irregular and short-crested waves.

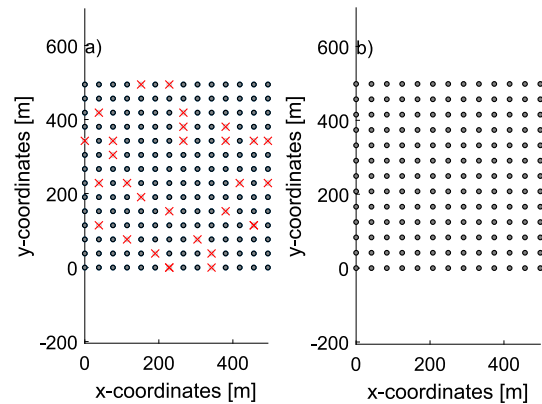


Fig. 1. Farm layout approximation used in the study. (a) Example of a farm of 200 WECs, with 30 WECs currently unavailable, shown as red crosses. (b) The modelled farm, where the remaining available WECs are distributed on a quadratic grid with a larger separation distance between the devices.

However, a more accurate description of the park interaction would need to account for the actual positions of the failed and available WECs, as well as the complete hydrodynamic interaction by scattered and radiated waves within the farm. Whereas this has been the topic of many of our and many other authors' previous works investigating optimal farm layouts (Götteman et al., 2015b, 2020), it is beyond the scope of the current paper.

The interaction between the WECs in the farm, and the resulting power absorption, is modelled using the simplified park interaction model derived by Stavropoulou and Götteman (2022). For clarity, it will here be reviewed.

With the given farm layout as a function of the number of available devices N , the average separation distance between WECs in the farm at any given time is

$$d = \frac{L_{park}}{\sqrt{N} - 1} \quad (9)$$

in units m. Note that it only makes sense to talk about a separation distance between devices when $N > 1$, hence the separation distance is positive and tends to infinity for $N \rightarrow 1$.

Assume that the irregular waves are long-crested and incident along the x -direction of the farm. The available energy flux is, for deep water, given in terms of the significant wave height H_s and energy period T_e of the waves as

$$J = \frac{\rho g^2}{64\pi} H_s^2 T_e \quad (10)$$

in units W/m. The available energy incident on a device of width D is thus DJ , and the capture width ratio in Eq. (8) is $\tau = P_{abs}/(DJ)$. A passive damping is assumed, such that the power take-off (PTO) damping can be adjusted to the current sea state. This means that the generator damping is adjusted once per hour to optimize the energy absorption in the varying wave conditions. The approach requires no wave forecasting (Götteman, 2022) and is more realistically feasible than an active control approach, although the latter can be used to obtain a higher energy absorption. The PTO damping and the computed absorbed power for a single WEC is shown for 10 days at the SE site in Fig. 2. The average power absorbed by the \sqrt{N} devices in the first row perpendicular to the incident waves is $\sqrt{N}\tau DJ$. Since the

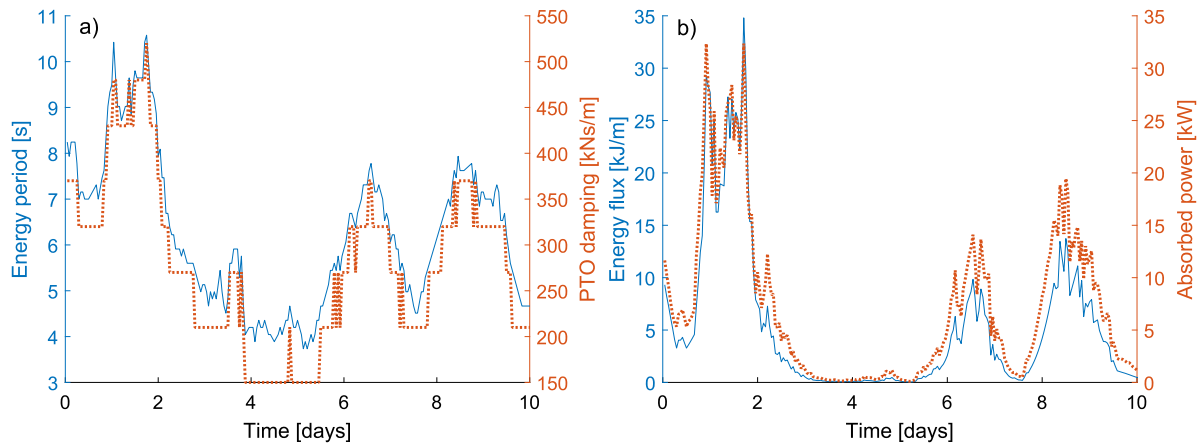


Fig. 2. (a) The PTO damping is modified to an approximately optimal value in each sea state, corresponding to passive damping. The figure shows energy period during 10 days at the SE site, and the corresponding PTO values. (b) The energy flux and the computed absorbed power of a single WEC during the same period.

power absorbed by the first row is not available to the second row, the available energy flux to row 2 is $J(1 - \tau D\sqrt{N}/L_{\text{park}})$. Consequently, the power absorbed by row 2 is $\sqrt{N}\tau DJ(1 - \tau D\sqrt{N}/L_{\text{park}})$. In general, it can be established that the power absorbed by row j is

$$P_{\text{abs,row } j} = \sqrt{N}\tau DJ \left(1 - \frac{\tau D\sqrt{N}}{L_{\text{park}}}\right)^{j-1}. \quad (11)$$

To this end, we introduce the parameter

$$s = 1 - \frac{\tau D\sqrt{N}}{L_{\text{park}}} \quad (12)$$

and notice that it satisfies $0 < s < 1$, that $D\sqrt{N}$ is the total width of all devices in a row, and that for few devices in the farm, $s \rightarrow 1$. The total power absorbed by the farm during each hour can then be obtained as a geometric sum over the \sqrt{N} rows,

$$\begin{aligned} P &= \sum_{j=1}^{\sqrt{N}} P_{\text{abs,row } j} = \sqrt{N}\tau DJ \sum_{j=1}^{\sqrt{N}} s^{j-1} \\ &= \sqrt{N}\tau DJ \frac{1 - s^{\sqrt{N}}}{1 - s}. \end{aligned} \quad (13)$$

Identifying the park interaction in expression (13) as

$$I = \frac{1 - s^{\sqrt{N}}}{(1 - s)\sqrt{N}}, \quad (14)$$

we can write the full power of the farm in terms of the park interaction as

$$P(t) = N(t)\tau(t)DJ(t)I(t). \quad (15)$$

In Eq. (15), the device width D is constant, whereas the capture width ratio τ , the number of available devices N , the incident energy flux J and the park interaction factor I may take different values each hour, which has been indicated by the explicit time dependence.

When the number of devices in the farm decreases, the park interaction tends to unity $I(t) \rightarrow 1$, implying that the interaction between the devices can be neglected and the power can be computed simply as $P = NP_{\text{WEC}}$, where the power of the individual WECs is $P_{\text{WEC}} = \tau DJ$. On the other hand, the park interaction I decreases with increasing number of available devices N , with increasing capture width ratio τ or device width D , and with decreasing farm area. The park interaction thus behaves as intuitively expected: it acts as a destructive shadowing effects which reduces the total power of the farm, an effect which grows with more densely populated farms, and it can be neglected when the WECs in the farm are few and separated by large distances.

2.2.2. Rated power

A realistic wave energy converter is subject to constraints in terms of maximal displacements, turbine velocities, or similar, restricting the dynamics and amounts of energy that can be absorbed. In this paper, the scope is not to model the dynamics of individual devices, as we aim to keep the discussion on a more general level. Instead, the upper constraint on performance is included in terms of the power rating.

Specifically, the WECs are given a certain power rating P_{rated} , and when computing the total hourly power of the farm according to Eq. (15), the power can never exceed the total rated power of the available devices. The full power of the farm is therefore computed according to Eq. (15) when this value is below the total power rating, and is otherwise set equal to the rated power at that time instant,

$$P(t) = \min\left(N(t)\tau(t)DJ(t)I(t), N(t)P_{\text{rated}}\right). \quad (16)$$

The effect of this constraint can be seen in Section 3 when discussing the total power of the farm over time. Whereas this constraint does not include a dynamical understanding of the upper limits of the energy absorption of the WECs, it excludes the unrealistic results that the energy absorption would simply grow with increasing energy flux J , without upper bound.

WECs come in different power ratings, and different dimensions may be suitable in different wave climates and locations (Pascal et al., 2018; Tan et al., 2021). To account for this, three different power ratings have been considered: 20 kW, 50 kW, 100 kW. These cover the usual range of power reported for small point-absorber WECs as studied in the current paper. In addition, in Section 3.6.1, an economic assessment will be carried out to find the optimal rated power in the range 0–100 kW at the two sites.

2.3. Repair operations and weather windows

Offshore sites can be accessed by different vessels and methods, each with their constraints and thresholds for when operations can be safely carried out. For instance, operations requiring divers have a different upper level for wave heights than operations with a heavy lift vessel or a rubber boat. The thresholds define *weather windows* – time periods when weather conditions are such that operations can be conducted, and conversely closed periods when repair cannot be carried out. During the closed periods, failed WECs cannot be repaired, as is implemented to evaluate the number of available devices in Eq. (24). The significant wave height is usually considered as a dominant threshold for offshore operations (Teillant et al., 2012; DNV, 2011). When lifting operation is required, the wind speed will also be important to ensure safe procedures.

It should be noted that some works have defined weather windows only with respect to the weather parameters (Gintautas and Sørensen, 2017; O'Connor et al., 2012; Martini et al., 2017), whereas others have taken into consideration also the specific offshore operation that is to be performed (Kennedy et al., 2017) or at least focused on the specific duration of the weather window (Silva and Estanqueiro, 2013; Walker et al., 2011). In this paper, the first definition has been used, to avoid restricting to certain operations or making assumptions on the type of failures and required duration of the weather windows. The weather windows definition used in the present paper is thus equivalent to the *approachability* of the wave farm. This approach provides a more generic analysis, but also a simplistic one. The complexity could be increased by analysing different kinds of failure modes, together with the time required for their repair operations, and the corresponding duration of weather windows.

Different vessels and their weather thresholds have been considered in reliability analyses of wave energy systems by O'Connor et al. (2012), de Andrés et al. (2015, 2016), Rinaldi et al. (2016b), Gueguen (2016) and Götteman et al. (2018). The thresholds range from maximal significant wave heights of $H_s \leq 1$ m for a “workboat” (Gueguen, 2016) or “unspecified vessel” (de Andrés et al., 2015) up to maximal wave heights of $H_s \leq 3$ m and maximal wind speed of $W_s \leq 15$ m/s for a HF4 (high-flow installation 4) vessel (Rinaldi et al., 2016b).

Common O&M strategies for offshore marine energy converters and offshore wind energy systems are:

- Crew transfer vessels are used for transferring technicians and small components with 26 knots maximum speed (Ioannou et al., 2018).
- Helicopters can transfer personnel and their equipment with maximum speed of 245 km/h (Ioannou et al., 2018).
- Diving support vessels are rented for underwater inspections (Ioannou et al., 2018).
- Jack-up vessels are used for heavy repair operations and component installations (Ioannou et al., 2018).
- Cable laying vessels are chartered for replacing the cables (Ioannou et al., 2018).
- Boats for carrying a remotely operated vehicle (ROV) or ROV vessel are chartered for remote underwater operation and inspections (Chatzigiannakou, 2019; Rémoit et al., 2018).
- Tugboats pulling a crane barge can transfer WECs to or from the site. A harbour crane is required in this case (Chatzigiannakou, 2019).

Table 2 summarizes different offshore vessel options with different weather threshold and day rates.

In this paper, the thresholds for maximal wave height and wind speed have been defined as $H_s \leq 1.1$ m and $W_s \leq 17$ m/s for the bulk of the analysis, corresponding to the “two tugboat and a crane barge” vessel specified in Table 2. To evaluate different repair vessel strategies and their impact on the resilience and economical viability of the system, the seven different vessel options specified in Table 2 are analysed in Sections 3.5–3.6. The effect of different threshold levels is further evaluated in a sensitivity analysis in Section 3.7.

2.4. Weather dependent failure rates

For structures such as wind turbines or buildings, the vulnerability to external weather hazards can be quantified in terms of fragility curves. These can be established by physical or numerical modelling. To develop a fragility curve, the first order reliability method (FORM) is an established method to assess the structural reliability of an object based on the probability of exceeding certain limit states at given environmental loads. For offshore wind turbines, fragility curves have been developed as functions on the wind and wave loadings, and used to assess the reliability and resilience of the systems (Pokhrel and Seo, 2019; Zuo et al., 2020). The same methodology will be applied here.

Table 2
Repair vessel options specifications.

Vessel type	H_s [m]	W_s [m/s]	Day/rate [k€/day]
Crew transfer vessel ^a	1.8 ^b	16 ^b	4 ^c
Jack-up vessel ^b	2 ^b	10 ^b	131 ^b
Helicopter ^d	99 ^d	20 ^d	5.5 ^d
Diving support vessel ^b	2 ^b	25 ^b	70 ^b
Cable laying vessel ^b	1 ^b	10 ^b	116 ^b
Two tugboat and a crane barge ^e	1.1 ^e	17 ^f	18 ^e
ROV Vessel + ROV device ^g	3.5 ^g	20 ^g	49 ^g

^aBard and Thalemann (2012).

^bSmart et al. (2016).

^cDalgic et al. (2014).

^dRademakers et al. (2009).

^eChatzigiannakou et al. (2014) and Chatzigiannakou (2019).

^fTraidMachinery (2022).

^gClarkson (2022).

As wave energy is not a mature energy technology, and there has been no convergence to a single or a few concepts, there are no fragility curves available in the literature for wave energy systems. Several papers have analysed and presented constant failure rates for wave energy systems. One recommended approach has been to use established failure rates for specific components and adjust them according to (constant) environmental and uncertainty parameters, by simply multiplying the known failure rates with estimated safety factors (Wolfram, 2006). Thies et al. (2009) computed failure rates for different components of the Pelamis WEC in this way, ranging from failure rates of the power transmission system of 0.47/year to the hydraulic power take-off system of 2.42/year. Cretu et al. (2016) established a failure rate of 1.9526/year for a linear generator, based on failure rates for some of the components. Failure rates of many components as well as subsystems were computed by a similar method by Ericsson and Gregorson (2018) for a point-absorber WEC with direct-driven power take-off. Based on the failure rates for subsystems, an overall failure rate for the WEC was computed in a fault tree analysis to 1.3186/year. The approach of using known failure rates for components and adjusting them is equipped with uncertainties, and a few papers have also presented failure rates of wave energy components based on experimental (Weller et al., 2015) as well as numerical works, mostly considering fatigue failures and adopting a rainflow analysis (Thies et al., 2011). However, few or no actual failure rates or fragility curves have been published as a function of wave loadings.

In this paper, we have therefore taken the approach of *constructing* a fragility curve as a function of the significant wave height. The fragility curve has been designed such that it gives plausible failure rates at calm and violent wave height conditions, based on the constant failure rates reported in the literature. Motivated by Kiel and Kjølle (2019) where time-dependent failure rates were seen to have a large effect on the predicted resilience of a power system, we will then use the varying failure rate to analyse the resilience of the system.

Let $f(x)$ be a probability distribution of the failure of a WEC unit due to an environmental parameter x , for instance on the form of a GEV distribution as in Eq. (1). The probability that the unit should fail in weather conditions $X < x$ is given by the cumulative distribution function in Eq. (3). Analogously, the probability that the unit will *not fail* in weather conditions $X < x$ is given by the reliability function, $R(x) = 1 - F(x)$. The instantaneous *failure rate* at weather conditions $X = x$ is given by the hazard function,

$$\lambda(x) = \frac{f(x)}{1 - F(x)}. \quad (17)$$

Note that since the weather conditions (here: the significant wave height) differ in time, the failure rate will be implicitly dependent on time, $\lambda = \lambda(x(t))$.

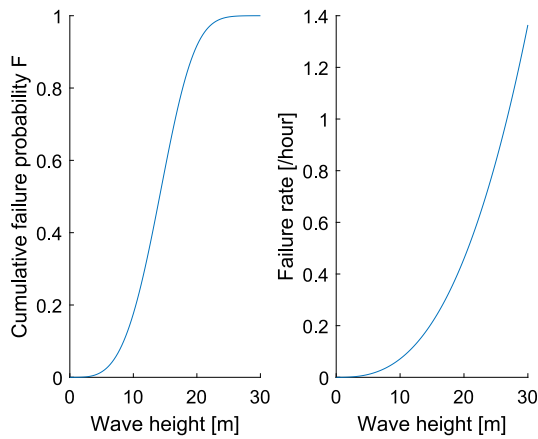


Fig. 3. Wave height dependent cumulative failure probability and failure rate used in the study.

Specifically, if the failure probability in terms of the wave height $x = H_s$ is given on the form of a 3-parameter Weibull distribution,¹

$$f(H_s) = \frac{k}{a} \left(\frac{H_s - b}{a} \right)^{k-1} e^{-\left(\frac{H_s - b}{a} \right)^k}, \quad (18)$$

the cumulative probability of failure up to wave heights H_s and the related reliability function will be

$$F(H_s) = \int_0^{H_s} f(H'_s) dH'_s = 1 - e^{-\left(\frac{H_s - b}{a} \right)^k}, \quad (19)$$

$$R(H_s) = e^{-\left(\frac{H_s - b}{a} \right)^k}. \quad (20)$$

From Eq. (17), the instantaneous failure rate of the WEC is

$$\lambda(H_s) = \frac{k}{a^k} (H_s - b)^{k-1}, \quad (21)$$

and the average failure rate during some time interval $[t_i, t_j]$ is then

$$\bar{\lambda}_{ij} = \frac{1}{t_j - t_i} \int_{t_i}^{t_j} \lambda(H_s(t_k)) dt. \quad (22)$$

A priori, the probability of failure and thus the failure rate may depend explicitly of both the time and the environmental parameters. The explicit time dependence is often modelled as a so called bathtub curve, with a decreasing failure rate in the early stages of the lifetime of the unit, a lower and approximately constant failure rate during the operational “useful life” of the unit, and increasing failure rate at the end of the life time. The higher failure rate in the early life stages (infant mortality) can be due to material defects, design mistakes or assembly errors, while the higher failure rate at the end of the life is due to wear out of the components, or fatigue. In this paper, we focus on the main, operational period, and do not consider fatigue or varying failure rates as a function of the age of the system. The failure rate will, however, be implicitly dependent on time, since it will be a function of the environmental parameters, which vary over time.

To construct a realistic failure probability $f(x)$, we assume that it takes the form of a Weibull distribution as in Eq. (18), as this is the standard form of representing failure probability distributions. Next, we require the failure rate of the full WEC in Eq. (21) to be 0.2/year in very calm conditions $H_s = 0.5$ m, and 3504/year in violent conditions, defined by wave height $H_s = 20$ m. In addition, we impose the requirement that the failure rate should be valid for wave

¹ Note that the expressions for the Weibull distributions in Eq. (1) and (18) have been defined differently, to agree with the standard definitions of the GEV and Weibull distributions. The two expressions are related by redefinitions of the parameters k , σ , and μ in terms of the parameters k , a , and b .

heights $H_s \geq 0$. These three constraints uniquely determine the three unknown parameters a, b, k in the distribution function Eq. (18), and the cumulative failure distribution in Eq. (19) as well as the failure rate in Eq. (21) can be determined as functions of the wave height, and are shown in Fig. 3. For reproduction purposes, the parameters are identified as $k = 3.69$, $a = 15.61$, and $b = -1.16 \cdot 10^{-16} \approx 0$, making it in practice a two-parameter Weibull distribution. Note that in Fig. 3, and from here on, the failure rate will be given in unit/hour, as this is the time step for computing the weather parameters and wave farm availability in the paper.

2.5. Weather dependent availability and resilience

2.5.1. Availability

Availability is defined as the ability of the energy system to operate as normal; consequently unavailability is the time when the system has failed and is waiting to be repaired or replaced, in other words the downtime. Availability is usually given as an average or converged constant value over an extended period of time, and measures the percentage of time that the system is able to operate as normal. Here, a time-varying failure rate is used, and the availability $A(t)$ will be a function of time. The number of available WECs is the farm that are able to operate as normal is thus $N(t) = A(t)N(t_0)$, where N_0 is the total number of WECs in the park. The average availability over a time period T is then the average of the instantaneous availability,

$$A = \frac{1}{T} \int_0^T \frac{N(t)}{N(t_0)} dt. \quad (23)$$

Kennedy et al. (2017) and Götteman et al. (2018) used constant failure rates to assess the availability of WEC systems as function of weather parameters and maintenance operations. A failure rate of 1.752/year was used by Kennedy et al. (2017) and it ranged between 0/year to 10/year by Götteman et al. (2018), with a particular focus on failure rate 1.752/year. Here, a similar approach will be taken, but instead of a constant failure rate, the failure rate will be weather depending (and thus time dependent), $\lambda = \lambda(H_s(t))$, based on the failure rate shown in Fig. 3.

The number of available (i.e., operational) WECs N_i in the farm at a given time step t_i is defined by the number of devices in the previous time step, minus the devices that failed during the time step, and plus the number of the devices that were repaired during the time step. Devices can only be repaired/reinstalled if offshore operations are allowed, i.e., during open weather windows T_{open} . Failures of the devices will occur both during open and closed weather windows (although the failure rate will be higher in violent weather conditions, which coincide with closed weather windows). The number of WECs N_i at time step t_i is thus

$$N_i = \begin{cases} N_{i-1}(1 - \lambda_i dt), & t_i \notin T_{open} \\ N_{i-1}(1 - \lambda_i dt) + (N_0 - N_{i-1})\mu_i dt, & t_i \in T_{open} \end{cases} \quad (24)$$

where the time step is dt , the initial number of devices is N_0 , and the failure and repair rates at time t_i are given by λ_i and μ_i , respectively. Note that, if repair rate was zero or equivalently there were no open weather windows available for repair, the number of devices would be strictly declining during each time step as $N_{i-1}(1 - \lambda_i)$. Similarly, if the failure rate is zero, the number of devices will be strictly increasing, up to a maximum of the initial number of devices N_0 .

In this paper, the repair rate is assumed constant with the value $\mu = 26$ /year, i.e., if there are 100 failed devices at a certain time, we assume that $100 \cdot 26 / 24 / 365 = 0.3$ of those are repaired during that hour. The downtime of the component between the moments when it fails and is back in operation is called mean time to repair (MTTR). In terms of the repair rate, it is defined as $MTTR = 1/\mu$. A repair rate of 26/year thus implies a mean time to repair of $1/26 = 0.04$ years, or 2 weeks. The chosen repair rate has been based on the study by Ericsson and Gregorson (2018), who analysed and evaluated repair rates for different

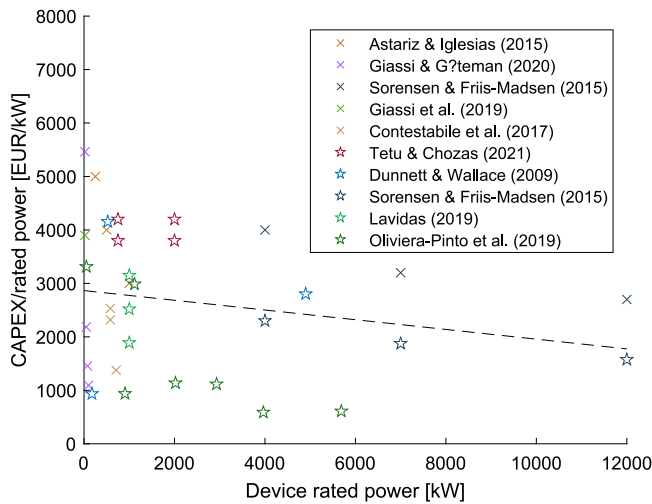


Fig. 4. CAPEX per rated power of WEC reported in the literature. Details are discussed in Section 2.6. Results for WECs in wave farm installations are shown with star markers; results for single-WEC installations shown with crosses.

types of failures of a similar point-absorber WEC. Different repair rates were also evaluated by Götteman et al. (2018), and the same repair rate of $\mu = 26/\text{year}$ was seen as a conservative yet realistic estimate of a generic failure.

2.5.2. Resilience metrics

To quantify resilience of power systems, either the availability in Eq. (23) or unavailability of the system can be used. Another common index is to use the expected energy not supplied (ENS), i.e., the amount of energy that was not delivered due to the disturbance. The index is sometimes given in units of kWh, and sometimes as a percentage of the total energy production had the disturbance not occurred (Espinoza et al., 2016). Here, the latter approach is used, and the percentage of the energy not supplied is defined as

$$\text{ENS}_{\%} = \left(1 - \frac{\int P(t)dt}{\int P^{\text{full avail.}}(t)dt} \right) \cdot 100, \quad (25)$$

where $P^{\text{full avail.}}(t) = \min(N_0 \tau(t) D J(t) I_0, N_0 P_{\text{rated}})$ is the absorbed energy at time t given full availability. Note that in the denominator, the energy flux $J(t)$ and the capture width ratio $\tau(t)$ are the only varying quantities, whereas the number of available devices $N_0 = N(t_0)$ and the park interaction $I_0 = I(t_0)$ are constant values. For the input parameter values as chosen in this paper, $N_0 = 200$, $I_0 = 0.849$, and the initial value of the parameter in Eq. (12) is $s_0 = 0.975$.

2.6. Economical assessment method and values

Since wave energy technology has not yet reached a commercial maturity, economical input values are equipped with large uncertainties. Published day rates for the vessels are shown in Table 2 and capital expenses (CAPEX) for WECs in Fig. 4. All vessel rates and the averaged CAPEX values are used as input to the present study. Due to the uncertainty in economical values for wave energy, the cost values will be compared to analogues from offshore wind.

Conversion rates used are 1 CDS = 0.70 EUR, 1 AUD = 0.63 EUR, 1 GBP = 1.16 EUR, and 1 USD = 0.88 EUR.

2.6.1. CAPEX

Dunnett and Wallace (2009) presented CAPEX for the AquaBuOY (point-absorber), Pelamis (linear attenuator), and WaveDragon (terminator) devices, rated at 250 kW, 750 kW, and 7000 kW each. The economical assessment was based on a 25 GWh wave farm at several

Canadian locations. In Canadian dollars, the costs were 935, 4155, and 2803 CDN/kW, respectively. The same results were used by Behrens et al. (2012) and Hayward et al. (2012) in a farm with total rated power of 21 MW (84, 3 and 28 devices).

Astariz and Iglesias (2015) used costs for three WECs with power rating 250 kW, 500 kW, 1000 kW as 5000, 4000, and 3000 EUR/kW. In addition, roughly the costs as in Dunnett and Wallace (2009) were used for the AquaBuOY (250 kW), Pelamis (750 kW) and WaveDragon (7000 kW), not duplicated in Fig. 4.

The techno-economic properties of seven WEC technologies installed in larger farms were assessed by Oliveira-Pinto et al. (2019). The rated power and CAPEX per WEC capacity were: bottom-referenced submerged heave-buoy, 906 kW, 937 EUR/kW; floating three-body oscillating flap, 5687 kW, 610 EUR/kW; floating oscillating water column, 2930 kW, 1116 EUR/kW; Pelamis, 1116 kW, 2987 EUR/kW; small bottom-referenced heaving buoy, 52 kW, 3312 EUR/kW; floating heave-buoy array, 3964 kW, 588 EUR/kW; floating two-body heaving converter, 2022 kW, 1137 EUR/kW.

CAPEX costs of 3899 EUR/kW were reported by Giassi et al. (2019) for a single point-absorber WEC with a rated power of 20 kW. The costs included installation, decommission and labour costs, but excluded costs for transmission and electrical equipment, as these were computed depending on the length of cables. In a subsequent paper, CAPEX values of 1093–5462 EUR/kW were reported for WECs with power ratings in the range 20–100 kW (Giassi et al., 2020).

Contestabile et al. (2017) computed CAPEX for the breakwater integrated overtopping WEC device OBREC. Two options for the power production were used: (1) a large number (125–675) of very small pico-turbines, with a nominal power of 1.5 kW each; (2) 3–5 larger Kaplan or screw turbines. 9 different configurations were considered for each option. Here, option (1) has been averaged as a single WEC with nominal power 711 kW, and option (2) as a single WEC with averaged nominal power 582 kW. CAPEX for the first option was 2185 AUD/kW, and for the second option 2531 AUD/kW or 2318 AUD/kW depending on if screw or Kaplan turbines were used. The CAPEX for the breakwater has not been included.

Based on 20 years development and scale tests in wave tanks and in the real sea, Soerensen and Friis-Madsen (2010) presented expected costs for a WaveDragon devices with rated power of 4, 7 and 12 MW to 4000, 3200 and 2700 EUR/kW. After deployment of 100 devices, these device costs were expected to reduce to 2300, 1875 and 1575 EUR/kW, respectively.

Some references have presented CAPEX costs without explicitly stating the rated power of the devices and/or the number of WECs in the wave farm installation. Three scenarios with a CAPEX of 3000, 4000, and 5000 EUR/kW were used by Lavidas (2019) for an wave energy installation of total 1 MW. Têtu and Fernandez Chozas (2021) presented CAPEX costs targets of 3800–4200 EUR/kW for an LiftWEC installation rated at 0.75–2 MW.

All CAPEX costs reviewed above have been collected in Fig. 4. The average of the data points is shown as a dotted line and used as input values to this study. As can be seen from the figure, the costs per kW reduce slightly for increased power rating.

To verify the costs estimations for wave energy installations reviewed above, comparisons to costs reported for offshore wind energy can be made. Vieira et al. (2019) discussed costs for European offshore wind turbines (OWTs), and reported average CAPEX for three turbine classes rated at 2.5, 3.8 and 6.9 MW as 3200, 3900, and 3350 EUR/kW. From those values, there is no trend that increased turbine size reduces cost per capacity. When studying the CAPEX for known offshore wind farms as function of total farm capacity, Vieira et al. (2019) found that the CAPEX/kW increases almost as a linear function with the capacity, except for very large farms where a scaling effect will reduce the CAPEX costs relative the linear trend. Such a scaling effect would agree with the ocean energy report of OES Ocean Energy Systems (2015), anticipating that CAPEX/kW will reduce significantly with

project capacity, but is to be validated in the future when more large farms have been commissioned. Vieira et al. (2019) also showed that the CAPEX/kW is generally lower for wind farms installed in shallower water (roughly 1250–4500 EUR/kW), than in deeper water (roughly 2000–5000 EUR/kW). In their NREL report, Stehly et al. (2020) listed CAPEX costs for onshore and OWTs. The total CAPEX of a fixed and floating 6.1 MW OWT was summarized as 4077 and 5328 USD/kW, respectively, of which the turbine cost was 1301 USD/kW.

When compared to Fig. 4, it can be seen that the CAPEX costs reported for offshore wind energy are in the upper, but same range as the ones reviewed above for wave energy systems. The average values used in the study (shown by dotted line in Fig. 4) can thus be viewed as a good, and possibly slightly optimistic, estimate for the CAPEX.

2.6.2. OPEX

Dunnett and Wallace (2009) presented operational expenses (OPEX) for AquaBuOY (point-absorber), Pelamis (linear attenuator), and Wave Dragon (terminator) as 0.069, 0.047, and 0.020 CDS/kWh, respectively. A yearly OPEX cost amounting to 5.5% of the initial CAPEX was assumed by Contestabile et al. (2017), whereas Têtu and Fernandez Chozas (2021) proposed 2.5%–4%, or annual OPEX values ranging between 65 and 340 EUR/kW. For the seven WEC technologies analyzed by Oliveira-Pinto et al. (2019), the OPEX for the wave farms were in the range 59–331 EUR/kW.

For offshore wind energy, annual OPEX costs of 124–130 USD/kW have been reported by Stehly et al. (2020). In the present study, the upper range of these values, 130 USD/kW, has been used as input value for the OPEX. This corresponds to 4% of the CAPEX costs, and is within the range of OPEX values typically reported and used for wave power systems.

2.6.3. FIT and discount rate

Feed-in tariffs (FIT) have been introduced to promote investments in renewable energy technologies and differ between different countries and over time. For instance, Vieira et al. (2019) reported that commissioning of relevant offshore wind capacity in Germany only started when the tariff rose from 91 to 150 EUR/MWh. An average of 110 EUR/MWh was used by Astariz and Iglesias (2015), and Contestabile et al. (2017) used a FIT of 40 AUD/MWh. A FIT of 250 EUR/MWh was reported in Lacroix et al. (2009) and has been used in several works (Giassi et al., 2019, 2020), and will be used also here.

A discount rate is used to assess the present day value of future costs and income. Contestabile et al. (2017) used a discount rate of 9%, and discount rates in the range 5%–10% were mentioned by Têtu and Fernandez Chozas (2021). Discount rates of 8% were reported by Chozas et al. (2014), Callaghan and Boud (2006), Ingram (2011), and also in the wave power assessment carried out in the NREL report by Black and Veatch (2012), and has been used in the present study.

2.6.4. Costs of repair vessels

To assess the economic performance of different repair options in the event of a harsh weather condition, the repair vessel costs are assessed, based on the vessel specifications given in Table 2 regarding weather thresholds and vessel costs, and compared to the energy not supplied. The day rate for each option is seasonal dependent, and here, only an approximate average rate is considered.

The cost for the repair vessels is computed as the cumulative costs of the hourly rate C_M of the vessel,

$$C_{\text{vessel}}(t) = \int_0^t f_{C_M}(\tau) d\tau \quad (26)$$

where $f_{C_M}(\tau)$ is the cost during each hour, which is zero if the vessel is not used,

$$f_{C_M}(t) = \begin{cases} 0, & t_i \notin T_{\text{open}} \\ C_M, & t_i \in T_{\text{open}} \end{cases} \quad (27)$$

Hence, the cost is accumulated only when the offshore site is accessible for repair.

2.6.5. Economical measures

Using the economical input values discussed in the previous subsections, financial quantities will be computed to evaluate different design and resilience strategies.

The net present value (NPV) is a quantity used to evaluate the profitability of a project. It is defined as

$$\text{NPV} = -\text{CAPEX} + \sum_{j=0}^{Y-1} \frac{E_{\text{annual},j} \cdot \text{FIT} - \text{OPEX}_j}{(1+r)^j} \quad (28)$$

where CAPEX is the total capital costs for the project, OPEX_j are the operational costs in year j , $E_{\text{annual},j}$ the annual energy production in year j , FIT the feed-in tariff, r the discount rate, and Y the expected lifetime of the project. The OPEX costs in Eq. (28) depend only on the installed capacity in the farm, and are independent of the vessel strategy chosen. The costs for vessels as defined in Section 2.6.4 are evaluated explicitly in Section 3.6.2.

The NPV is computed in Section 3.6 and used to evaluate the feasible power rating strategies at the two sites.

To evaluate the repair strategies from an economical perspective, quantities computed over the whole lifetime of the farm are not suitable. Instead, the energy not supplied after a disruptive event can be given an economical measure in terms of the cumulative cost of the energy not supplied,

$$C_{\text{ENS}}(t) = \int_0^t (P^{\text{full avail.}}(\tau) - P(\tau)) \cdot \text{FIT} d\tau \quad (29)$$

where, according to Eq. (25), $P^{\text{full avail.}}(t)$ and $P(t)$ are the power produced at time t for a farm with full and reduced availability, respectively. The cost of the energy not produced can then be valued against the cost for repair vessels in Eq. (26).

2.7. Numerical implementation

The theory and methods described in the above subsections has been implemented in a MATLAB script and simulations have been carried out on a standard desktop PC. For the extreme weather characterization, the weather data for the US site was available on an hourly basis, whereas for the SE site the sampling frequency was 1/h for the wave data but 0.25/h for the wind data in the first 10 years 1976–1986, after which the frequency increased to 1/h. The wind data at the SE site was therefore interpolated to an hourly interval for the first 10 years of data.

3. Results

3.1. Extreme weather characterization

The annual maximum value of the average wind speed and significant wave height (both computed over one hour, and thus do not represent the actual maximal wind speed or wave height) have been identified and are shown in Fig. 5 for the two sites. The annual maxima are roughly in the same interval for the two sites, but a few larger wave height extremes can be seen for the US site, and a few lower wind speed values can be seen for the SE site.

According to the block maxima method reviewed in Section 2, the annual extremes for average wind speed and significant wave height have been fitted to generalized extreme value (GEV) distributions, according to Eq. (1) and (2). The parameters defining the GEV distributions are listed in Table 3. For the SE site, the shape parameters for the wave height and wind speed are negative, showing that their extremes are best described by a Weibull distribution. For the US site, the shape parameter is close to zero (although slightly positive for the wave height and negative for the wind speed), showing that the wind speed and wave height can be approximately described by a Gumbel distribution. The Gumbel distribution is skewed to the left as compared to the Weibull distribution, which is skewed to the right. This indicates that most extreme values at the US site are found in the upper tail of

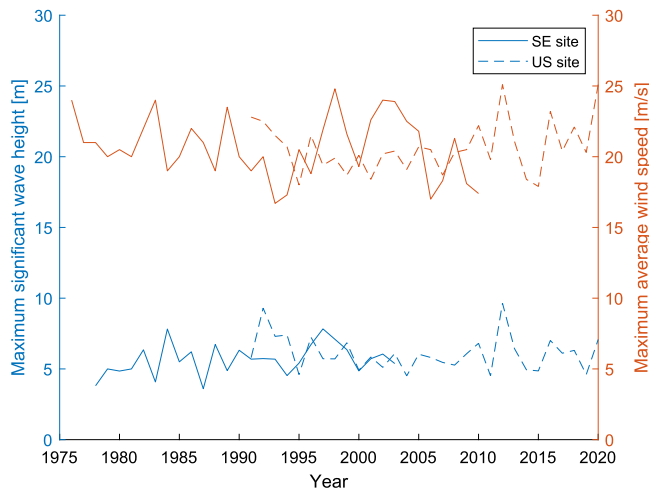


Fig. 5. The annual maximal wind speed (average over 1 h) and significant wave height at the two sites. The SE site is shown with solid lines, the US site with dashed lines.

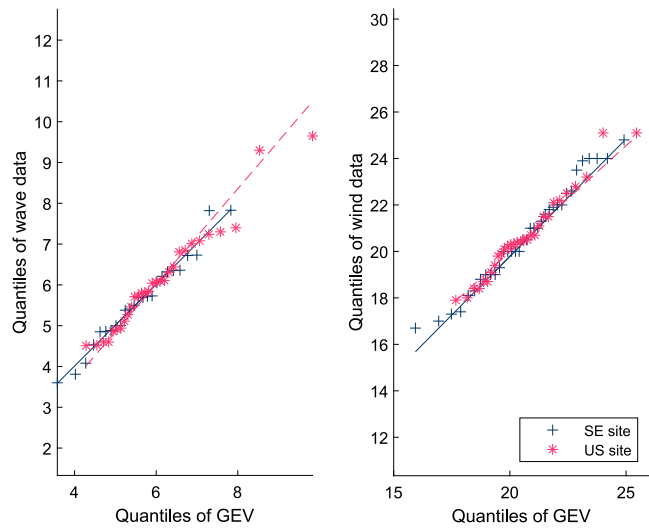


Fig. 6. Quantile–quantile plot for wave and wind data at the two sites. The SE site is shown in dark blue colours and solid line, the US site in red colours and dashed line.

Table 3 Identified parameters in the GEV distribution for the annual significant wave height H_s and hourly average wind speed W_s maxima.

Parameter	SE site		US site	
	H_s GEV	W_s GEV	H_s GEV	W_s GEV
Shape k	-0.230	-0.332	0.0672	-0.0414
Scale σ	1.018	2.172	0.918	1.492
Location μ	5.209	19.970	5.518	19.841

the weather population, whereas they are found in the lower tail at the SE site. Expressed differently, the wave heights and wind speeds corresponding to the same return period T_R are expected to be higher at the US site, as compared to the SE site. Similar conclusions were obtained by Jonathan and Ewans (2007) when comparing extreme wave heights at locations in the Gulf of Mexico and the Northern North Sea.

To analyse the goodness of fit, quantile–quantile (qq) plots are shown in Fig. 6 for the two sites. Fig. 6 shows that the extreme wave and wind data follow the GEV distribution defined by the parameters in Table 3 well at the SE site. For the US site, the fit is also satisfactory, but some deviations in the highest quantiles can be observed.

Table 4

Weather windows T_{closed} closed for repair according to weather thresholds $H_s \leq 1.1$ m and $W_s \leq 17$ m/s, average failure rates $\bar{\lambda}$, and percentage of time when the failure rate λ is lower than the average failure rate, computed at the two sites for the year of focus.

Site	Year	T_{closed}	$\bar{\lambda}$	$\lambda < \bar{\lambda}$
SE site	1984	76 days	1.25/year	83%
US site	1996	178 days	4.13/year	81%

To compare the extreme weather conditions at the two sites, the return periods and corresponding extreme values are computed, according to Eq. (6), or, equivalently, by Eq. (7). The return periods of $T = 10, 25, 50, 100, 1000$ years are evaluated, and the corresponding maximum significant wave height and hourly average wind speed are shown for the two sites in Fig. 7.

As could be apprehended from the slightly higher maximal annual wave heights at the US site and the slightly lower annual wind speeds at the SE site (shown in Fig. 5), the weather is predicted to be more extreme at the US site, with weather parameter values corresponding to the same return periods. In particular, this holds for the long return periods of 1000 years or more. It should be remembered, however, that the uncertainty in the prediction increases with the return period, as only a limited amount of data have been used for the extreme value analysis.

3.2. Weather windows and failure rates

To study the weather dependent failure rates and performance of the farm, one year of data have been analysed in more detail at both sites, as described in Section 2. According to the hourly wave and wind data and the defined thresholds for offshore operations, weather windows closed for repair have been identified, and are shown as grey shaded areas in Fig. 8. For clarity, a zoom of the first 30 days at each site is shown. During these days, it is clear that the US site has fewer time slots available for repair operations, than the SE site. The same trend holds throughout the year as is also reported in Table 4: at the SE site, 76 days are closed for repair operations this particular year (and with the chosen weather thresholds), whereas the corresponding number for the US site is 178 years, i.e., almost half of the year.

As the next step, the weather dependent failure rates are computed during each hour according to the instantaneous failure rate (hazard function) given in Eq. (21) and shown in Fig. 3. Note that the failure rates for the WECs are computed as functions only of the (time-varying) wave height, whereas the weather windows are functions of both the wave height and wind speed. The rationale is that the wind speeds affects the WEC device to a smaller degree than the offshore vessel sea keeping and offshore repair operations.

The resulting varying failure rate as well as the significant wave heights at the sites are shown for the full year in Fig. 9 for both sites. It is clear from the figure that the failure rates increase with increased wave height, and that some instances of violent wave conditions give rise to peaks in the failure rate. The average of the failure rates are shown in Fig. 9 as black dotted lines, and can be seen to be higher at the US site than at the calmer SE site. The average failure rates are listed in Table 4 and amount to 0.000143/h, or 1.25/year, at the SE site, and to 0.000472/h, or 4.13/year, at the US site. As can also be anticipated from Fig. 9, during most of the year the failure rate is below the average. Indeed, at the SE and US sites, the percentage of the time when the failure rate is below the average failure rate, $\lambda(H_s(t)) < \bar{\lambda}$, is 83% and 81%, respectively. Only during times of storms and harsh weather conditions is the actual failure rate higher than the annual average. The developed method thus gives realistic results; the obtained average failure rates are in the same range as those reported in literature, but higher failure rates are obtained in severe metocean conditions.

From the computed time-varying and average failure rates, the reliability function can be derived as a function of time, according to

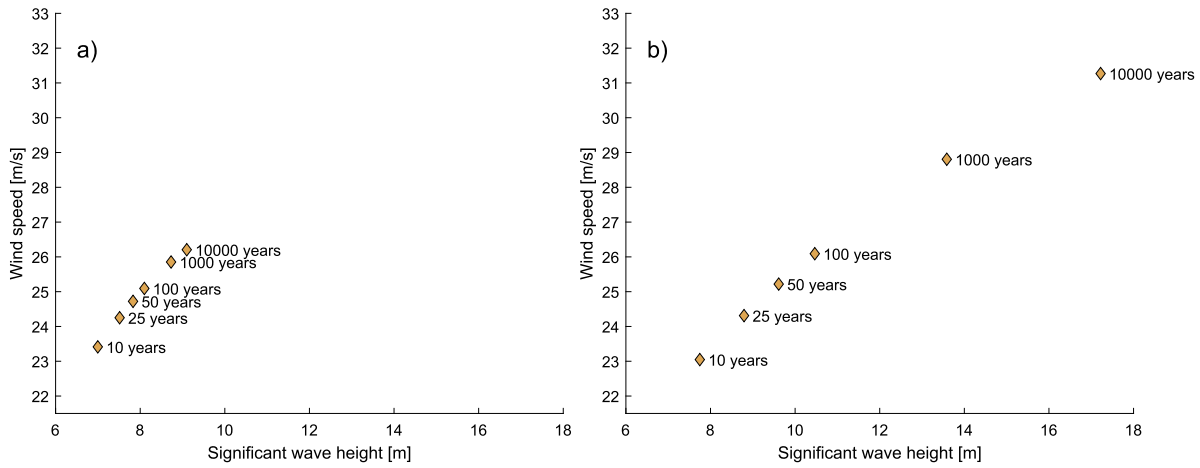


Fig. 7. Return values for significant wave height and average wind speed for different return periods. (a) SE site; (b) US site.

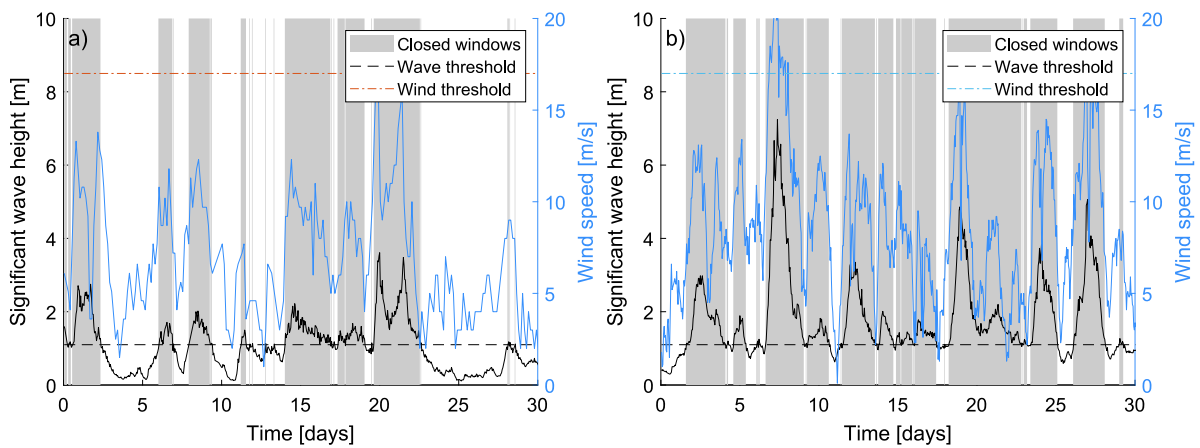


Fig. 8. The metocean parameters during 30 days. Repair operations cannot be carried out when the parameters are above the thresholds $H_s^{\max} = 1.1$ m or $W_s^{\max} = 17$ m/s (shown as grey shaded areas). (a) SE site; (b) US site.

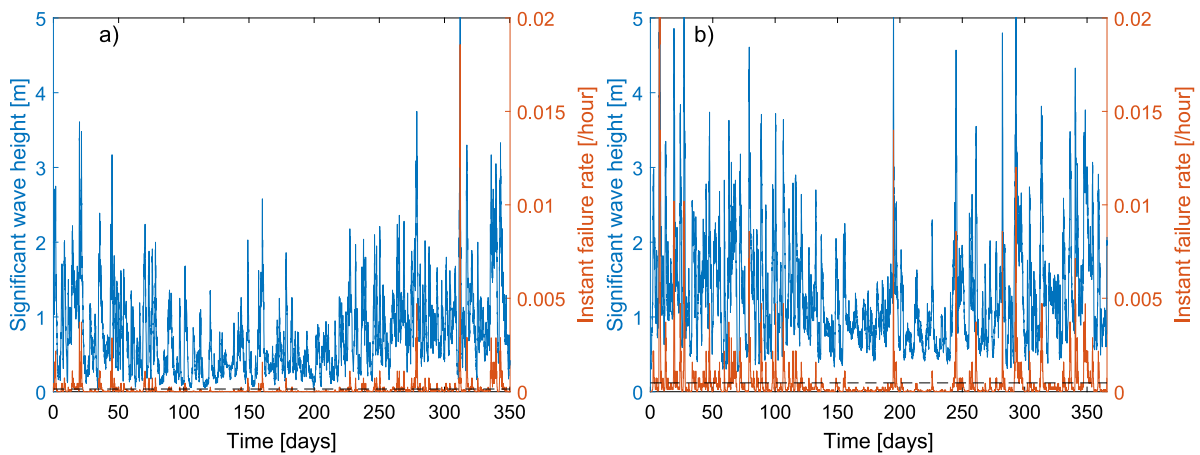


Fig. 9. The weather dependent failure rates at (a) SE site; (b) US site. The average failure rate is shown by dashed black line.

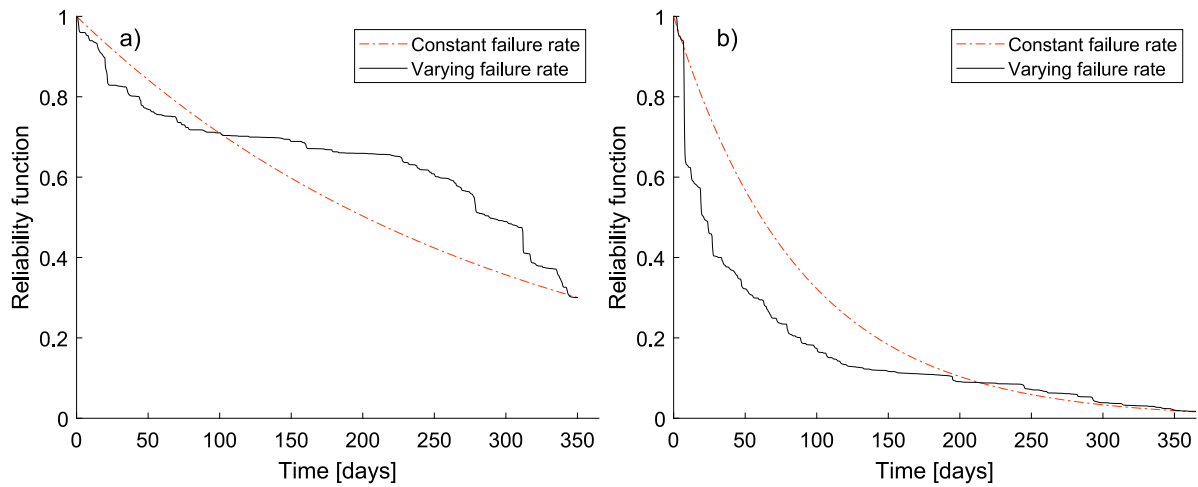


Fig. 10. The reliability function computed with weather dependent (“exact”) and constant failure rate (“approximate”) at sites (a) SE site, (b) US site. Note that no repair is considered.

Eq. (20) where the wave height is a function of time, $R = R(H_s(t))$. Eq. (17) for the failure rate can be rewritten as

$$\lambda(t) = \frac{f(t)}{1 - F(t)} = \frac{-R'(t)}{R(t)} = -\frac{d}{dt}(\ln(R)) \quad (30)$$

from which it follows that the reliability function can be expressed in time in terms of the instantaneous failure rate as

$$R(t) = e^{-\int_0^t \lambda(\tau) d\tau}. \quad (31)$$

The computed reliability is shown in Fig. 10 for the two sites. In solid black is the reliability function computed for the instantaneous failure rate throughout the year, and in dotted red is the approximation when the failure rate is the average (22) over the time interval $[0, t]$. Note that no repair is considered in Fig. 10; it is the decreasing reliability of a WEC over time, if no repair is carried out. From the figure, it can be seen that the milder wave climate at the SE site results in a reliability function that is decreasing more slowly, than at the site NBDC with harsher wave conditions.

3.3. Weather dependent availability

The reliability in Fig. 10 is computed without considering repair of the devices, and is therefore strictly decreasing. To compute the actual number of available WECs in the farm throughout the year, Eq. (24) should be used, which includes repair of failed devices whenever the metocean conditions allow for repair operations, $t \in T_{\text{open}}$. The result can be seen in Fig. 11 for the two sites. When comparing to the reliability in Fig. 10, it is clear that the number of devices increase during open weather windows.

In Fig. 11, the number of available devices is shown both for the time-varying failure rate $\lambda(t)$, and also for the case when the failure rate is approximated by the constant yearly average failure rate $\bar{\lambda}$. As was reported above, during the majority of the year, the weather is calm and the actual failure rate is below the average failure rate. This implies that during calm weather, the number of WECs computed with the average failure rate overpredicts the number of failures, whereas they are underpredicted during periods of harsh weather. This can be clearly seen in Fig. 11, where the constant failure rate gives a less dynamic prediction of the number of available WECs in the farm.

From the results of the number of available WECs shown in Fig. 11, the availability can be computed according to Eq. (23). The average availability of the year is shown in Table 5, and amounts to 95% for the less energetic SE site, and 76% for the high resource US site.

3.4. Weather dependent power production

3.4.1. Park interaction

The US site will be used to illustrate the effect of the park interaction model and the power rating constraint. In Fig. 12, the total power of the farm (computed as hourly averages) is shown for the US site at power rating 50 kW. For clarity, only the first 30 days of the year are shown. The power is computed according to Eq. (16), i.e., the total number of available WECs (shown in Fig. 11) is multiplied with the energy absorbed by each WEC, and with the park interaction factor in Eq. (14). If the power exceeds the allowed level, which is defined as the number of available devices operating at their rated power, the total power of the farm is defined as the maximal allowed, $N(t)P_{\text{rated}}$. The effect of the upper constraint for the absorption can clearly be seen in Fig. 12; the value $N(t)P_{\text{rated}}$ at each time step is indicated by the blue dotted line, and the total power is defined such that it never exceeds this value.

The effect of the park interaction can also be seen in Fig. 12. If interaction between WECs was neglected, the total power would be equal to the “ P_{tot} no interaction” seen in the figure. This value is slightly higher than the actual total power including the park interaction, which is to be expected. The park interaction in Eq. (14) decreases with number of available WECs in the farm, and in this particular example takes values in the range 0.849–0.913 over the year.

3.4.2. Power production and annual energy

In Fig. 13 it can be seen that the assumption of a constant failure rate gives a slightly higher prediction of the power production of the farm, in particular during times of high power production, i.e., during energetic wave conditions. This is to be expected, as the constant failure rate will overpredict the failure rate in calm conditions (leading to fewer available devices than in reality), and underpredict the failure rate in high wave conditions (leading to more available devices than in reality). In highly energetic conditions, the constant failure rate thus predicts a higher power production, whereas the power production in calm conditions is already low and therefore less affected. In other words, a constant failure rate only sees the positive aspects of high waves (higher energy absorption), whereas a more realistic weather-dependent failure rate balances the positive aspects with the negative (higher probability of failures). This can be further seen in Table 5 for both sites evaluated during one year at different power ratings of the WECs. In all cases considered, the assumption of a constant failure rate gives a slightly higher prediction of the annual absorbed energy, as could be seen also in Fig. 13. The difference between using a varying and constant failure rate for the annual energy absorption is 2%–7%.

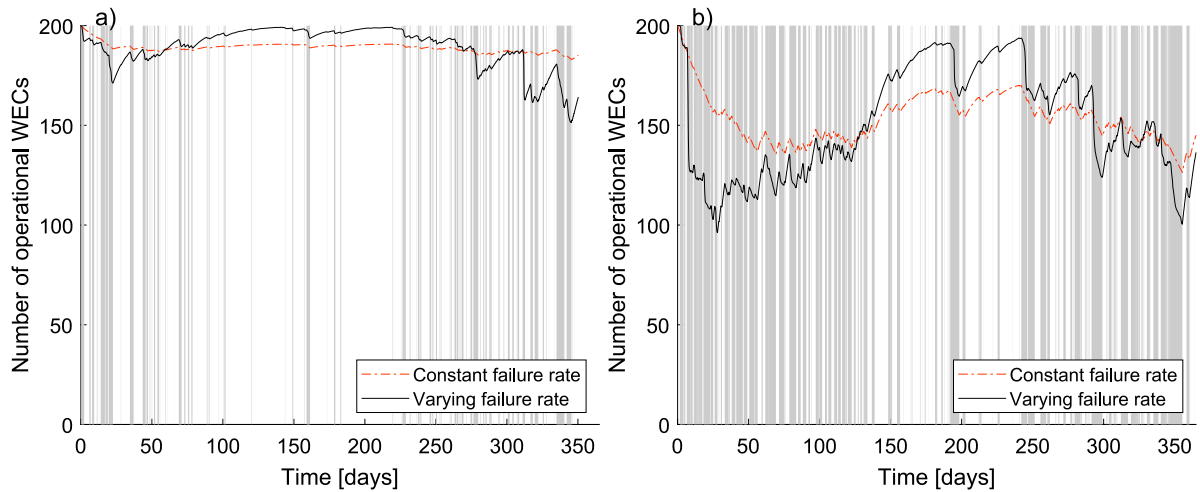


Fig. 11. Available WECs in the farm during a year at sites (a) SE site; (b) US site. Repair rate 0.0030/h is assumed. The time varying failure rate of Fig. 9 is compared to the situation with constant (time-averaged) failure rates. The grey shaded areas represent periods closed for repair operations.

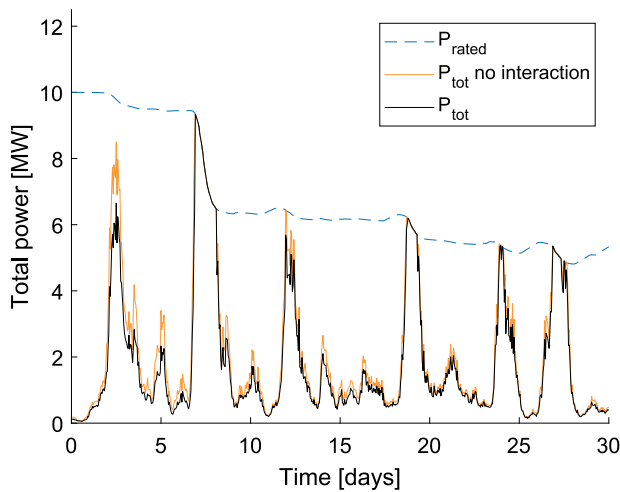


Fig. 12. Total power in the farm computed with and without interaction between WECs, according to Eq. (15). The US site at power rating 50 kW is considered.

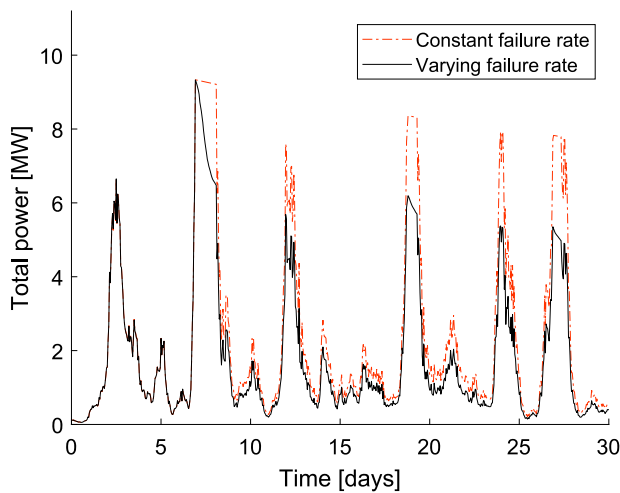


Fig. 13. Total power in the farm, when the available number of WECs in the farm have been computed according to a time-varying and constant failure rate, as in Fig. 11. The US site at power rating 50 kW is considered.

Table 5

Average availability and annual energy absorption at the two sites. The energy absorption is shown at different power ratings (20, 50, 100 kW) of the WEC, and shown for both the weather dependent and constant failure rates (the latter results shown in parenthesis).

Site	A	E_{annual} [GWh]		
		20 kW	50 kW	100 kW
SE site	95%	5.04 (5.16)	5.30 (5.44)	5.36 (5.50)
US site	76%	8.57 (9.11)	10.10 (10.78)	10.48 (11.21)

Whereas this might seem small, overestimating the energy absorption by a few percentages can have a large impact on the electric grid balance if the penetration of wave power was larger than today. Also, the difference is larger for the more energetic US site, and it can be expected that the difference will be even larger for more energetic sites.

3.5. Wave farm resilience

The resilience of the system can be quantified in terms of the energy not supplied, defined in Eq. (25). For the three different power ratings, the ENS at the SE site is in the range 10.5–11.4%, whereas at the US site it is in the range 13.5–18.5%. The power rating thus does not affect the resilience to a large degree, and it can be seen that the SE site has a higher resilience in terms of the ENS.

As can be seen from Fig. 11, a disruptive event such as the one occurring on day 7 at the US site can impact the full performance of the farm for a long time. With the vessel options considered in Fig. 11, almost 200 days are required before the farm has been repaired to its original function. The scenario causing the large disruption is the extreme wave height $H_s > 7$ m seen in detail in Fig. 8. From the return periods shown in Fig. 7, it is clear that such extreme wave heights are expected to occur more often at the more energetic US site, than at the calmer SE site. The expected maximal significant wave height corresponding to return periods 10, 25, and 50 years at the two sites is 6.70 m, 7.51 m and 7.83 m for the SE site, and 7.74 m, 8.79 m and 9.61 m for the US site. Large disruptive events can thus be expected to occur more often at the US site, and should be matched with vessels capable to operate in harsher weather.

To investigate strategies to improve the resilience of the park, the availability of operational WECs considering different repair options is shown in Fig. 14. At both sites, a disruptive event occurs during the first month. This event is particularly disastrous at the US site, where the availability drops by over 30%. The recovery after the events at both sites using different vessels is shown during the first 180 days.

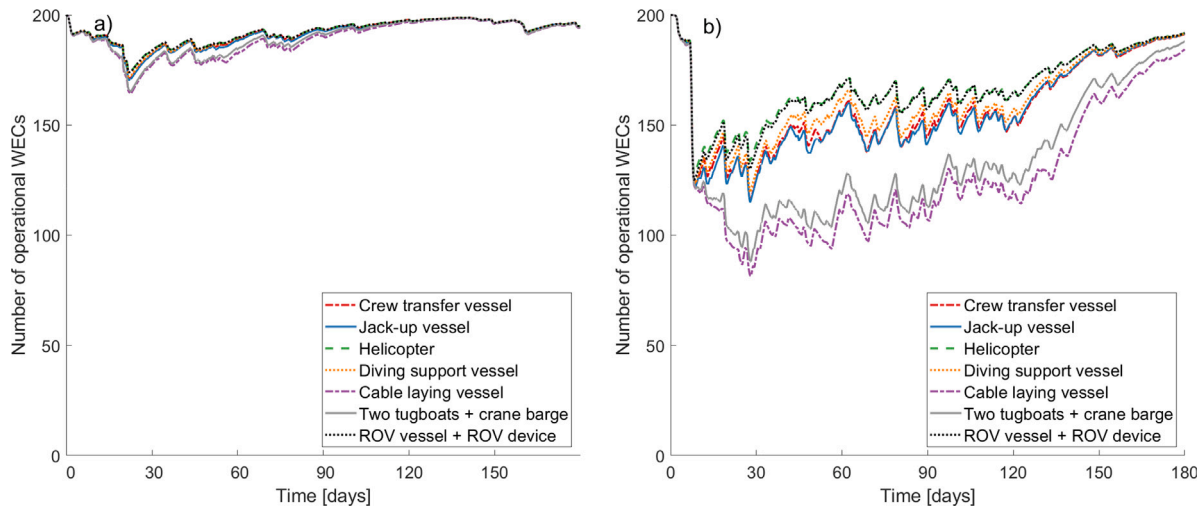


Fig. 14. The number of available WECs in the park during a year at sites (a) SE site; (b) US site for different vessel options with different weather thresholds.

From Fig. 14 it is clear that the choice of repair vessels has a large impact on the recovery process after an event, in particular at sites with limited weather windows. At the US site, the cable laying vessel and the two tugboat + crane barge result in a slower recovery process, due to their more restrictive weather thresholds. The significant wave height is seen as the most influential parameter in defining the threshold for repair operations. This can be observed when comparing jack-up and diving support vessels.

3.6. Economical assessment

3.6.1. Rated power

The annual energy absorption at the two sites for WECs with power rating 0–100 kW (total farm capacity 0–20 MW) is shown in Fig. 15. As expected, larger WECs with larger rated power lead to increased annual energy absorption. However, after certain rated power levels, the increase in annual energy is small. This leads to the question if there is an optimal power rating that can be identified, and if it differs between the two sites.

Based on the literature review for wave and wind energy installations in Section 2.6, the capital costs increases with the rated power and is usually given in units EUR/kW. The CAPEX per capacity cost is not constant, but seems to reduce slightly for larger installations, as seen in Fig. 4. Using the economical input values defined in Section 2.6, the NPV has been computed according to Eq. (28) and is shown in Fig. 15 as function of power rating. The NPV is positive in lower ranges of power rating. In other words, when increasing the WEC size above certain limits, the extra costs are not met by sufficiently increased energy absorption.

The feasible power ratings are different at the two sites. At the SE site, the NPV is positive for WECs rated ≤ 16 kW, and reaches a maximum value of 5.0 MEUR at power rating 5 kW. At the US site, the NPV is positive for WECs with rated power ≤ 31 kW, and reaches a maximum value of 9.6 MEUR at power rating 10 kW. Thus, the installations show a potential profitability at both sites, and small, cheaper WECs are the preferred strategy.

These results should be understood from the context of the mild wave climate at both sites; in particular the SE site which represents an extremely calm wave climate. The annual energy absorption at both sites is roughly in the range 5–10 GWh. This can be compared with the wave energy absorption for similar wave farms in the Baltic Sea, as computed by Engström et al. (2020). There, a total energy absorption 4–8 GWh was obtained at calm locations comparable to the ones studied in this paper, but 16 GWh was obtained at the most energetic sites. At such energetic sites, WECs with higher rated power would be preferred, than the ones obtained here. This is further discussed in Section 4.

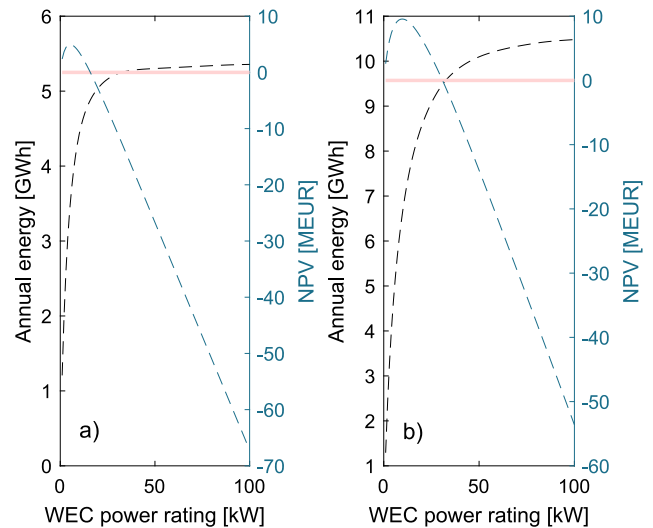


Fig. 15. Annual absorbed energy as function of the rated power of the device in the park at sites (a) SE site; (b) US site, shown as dotted line. The NPV is computed using Eq. (28) and the economical input values defined in Section 2.6, and shown for different power ratings as solid line.

3.6.2. Vessel strategies

To investigate the resilience of the park from an economic perspective, the costs of the ENS in Eq. (29) are analysed in relation to the costs of vessel strategies in Eq. (26). The ratio of the two costs is shown in Fig. 16 for the same 180 days as shown for the availability in Fig. 14.

Interesting conclusions can be drawn from Fig. 16. First, it can be seen that for the SE site, the costs of the repair vessels significantly exceed the costs of the ENS. In other words, it is more costly for a wave farm developer to repair the WECs, than to leave them failed in the ocean. The reasons for this is that the availability of the SE site is still high, and that the vessel costs are high in relation to the energy production of the WECs.

At the US site, the situation is different. Due to the many failed devices during the first month, the cost of the ENS is higher than the cost of some of the repair strategies. In particular, the cost of the crew transfer vessel and the two tugboat + crane barge are both lower than the cost of ENS. The cheaper day rate of the crew transfer vessel makes it economically advantageous over other options. However, in this economical model, the mean time to repair (MTTR) is considered constant. In other words, the downtime of the WECs are only affected

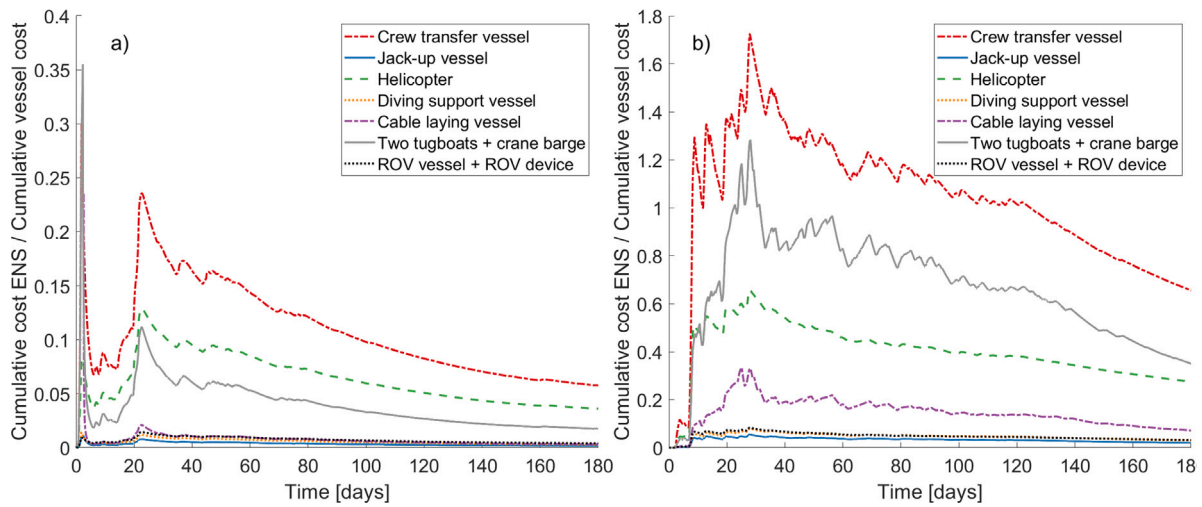


Fig. 16. Ratio between cost for ENS and vessel cost for different vessel options for rated power of 50 kW and duration of 180 days for sites (a) SE site; (b) US site.

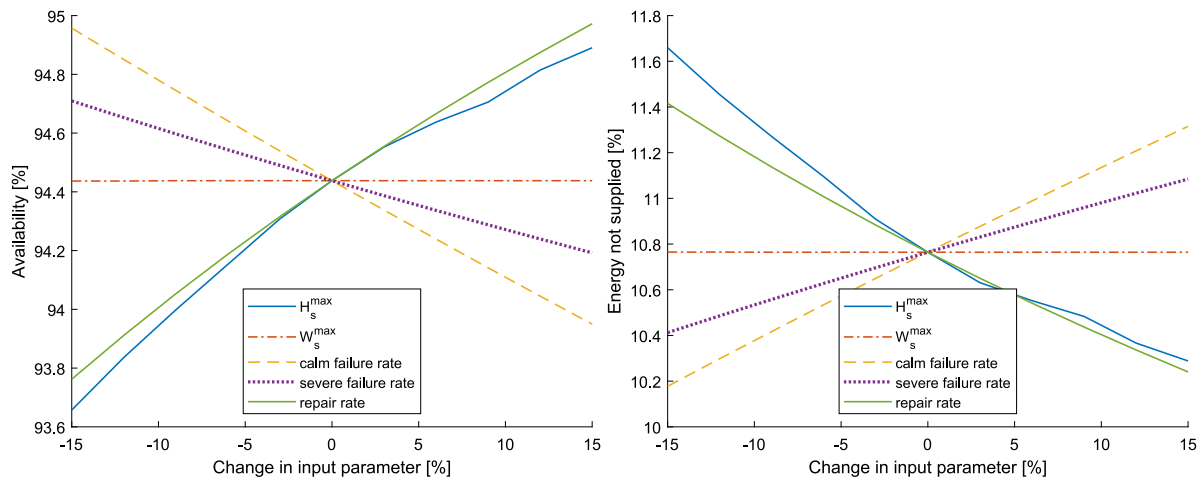


Fig. 17. Sensitivity analysis of the availability, taken as average over the year and shown as percentage of full availability, and the energy not supplied (ENS) to the input parameters for the SE site at power rating 50 kW.

by the weather limits of each vessel and the parameters such as the transit time from port to the site and how fast the repair operation is performed are not considered. In the first few days of the SE site, the significant wave height shown in Fig. 16 is higher than the operational limit for most of the repair vessels which implies zero repair cost (see Eq. (27)) during these days and results in the peak in the ratio between the cost of ENS and cost of vessels.

When comparing Figs. 14 and 16, it can be seen that the recommended vessel strategy is not always the one that gives the highest availability, and also not always the one with the lowest day rate. Since the produced power by the WECs depends on the energy flux which varies over time, the situation is more complex and must be analysed using economical metrics, as in the method presented here.

3.7. Sensitivity on input parameters

To study the sensitivity of the method to the choice of input parameters, a sensitivity analysis has been carried out. In Fig. 17, the availability and the ENS has been computed with a range of five different input parameters, where the default values are $H_s^{\max} = 1.1$ m, $W_s^{\max} = 17$ m/s, and the repair rate is $\mu = 26$ /year. The calm and severe failure rate are the input values chosen to define the fragility curve

in Fig. 3, where a failure rate of 0.2/year was assumed in very calm conditions $H_s = 0.5$ m, and 3504/year in violent conditions, defined by wave height $H_s = 20$ m.

As can be seen from Fig. 17, increasing the wave thresholds H_s^{\max} implies that the availability increases while the ENS decreases, which is expected as increased thresholds will allow for more repair operations. Increasing the wind threshold W_s^{\max} has negligible effect, since the wind speeds at the site are in general lower than the high threshold 17 m/s. Increasing the assumed values for failure rates at calm and severe conditions reduces the availability and increases the ENS, and likewise increasing the repair rate will increase the availability and reduce the ENS. Even when changing the input values $\pm 15\%$, the resulting availability and ENS change by less than 0.8% and 8%, respectively. The method is thus little sensitive to the choice of input parameters.

4. Discussion and future work

To understand the availability of a system due to weather conditions and repair strategies, one must analyse not only the weather parameters, but also have reliable models and input values for probability of failures, the performance of the system in different conditions, and the possible offshore vessels. All of these input parameters are difficult to

obtain for a technology that is not yet mature, and where very little data is publicly available. In this paper, the strategy has been to use the input data that is available, and construct the others based on experience and on data for related systems.

An assumption used in the paper is the simplified park interaction developed in this work. Future work could attempt to model the park interaction within the park accurately instead of the approximate interaction in Eq. (14) and the approximate layout shown in Fig. 1. To model the accurate power absorption, irregular waves should be used as input, and the full dynamics of the park should be modelled, including the response to scattered and radiated waves. At present however, such an approach is not realizable due to the high computational cost, even with weak approximations such as an interaction distance cut-off (Göteman et al., 2015b), or with access to high performance computer clusters. The annual energy obtained in this paper, using the simplified park interaction factor, is in the same range as for the comparable sites and wave farms studied by Engström et al. (2020). Since the energy absorption was computed with a more advanced hydrodynamical interaction model in Engström et al. (2020), the agreement serves as a consistency check for the simplified farm model applied here.

The method is scalable for wave farms of any size. Here, a farm size of $N = 200$ was chosen, as this is a realistic size of a fullscale installation of small point-absorbers. Applying the method to a single WEC would not be of much interest, since the number of devices in the park could then take only two values – 0 or 1 – and the power production from the park would be either zero or equal to that of a single WEC.

Long-term predictions of weather parameters are bound with uncertainties. As the objective of the extreme value analysis is to analyse the tail of a distribution, and not the body of it, typically only a very limited amount of data samples are available, and extrapolation beyond the sample size is needed (Jonathan and Ewans, 2013). Maximum likelihood estimators (MLE) can be used to determine the minimum sample size required for different return periods (Cai and Hames, 2010), based on the idea that the MLE are normally distributed for a large enough sample size. Cai and Hames (2010) found that the sample size required to predict 100 year values accurately differ between different data types (e.g. sea levels and temperature), and ranged between 44 and 72 years. The weather data at the two sites have been accumulated during 19 years at the US site and 14.5 years (wave data) and 26.5 years (wind data) at the SE site. However, at both sites there are several time regions of missing and erroneous data, and data points of higher wind speeds and wave heights might have been missed. The sample size is thus considerably smaller than recommended by Cai and Hames (2010) for accurate prediction of 100-year return values, but larger samples of data are seldom available. The qq-plots shown in Fig. 6 still induce trust in the accuracy of the results, in particular for the return periods ≤ 50 years, but results for return period values > 100 years shown in Fig. 7 should be interpreted with caution. As a complement to available weather data, future work could also apply wave-wind hindcast models to assess long term weather statistics, such as the WAVEWATCH III used to obtain wave and wind data around Ireland by Gallagher et al. (2016), or the WAM model used by Wrang et al. (2021) to obtain extreme weather statistics at offshore sites.

The extreme wave and wind data have here been analysed by independent distributions, and the vulnerability of the WECs have been assumed to depend only on the wave height, and not the wind speed. This could be generalized to a multivariate extreme value distribution for both wind and wave extremes, to provide extreme contours for the different extreme value parameters. For the wave extremes, not only the wave height could be considered, but combinations of wave height and periods. When analysing vulnerability in terms of both wind and wave loadings, as would be appropriate for floating offshore wind turbines, a joint distribution should preferably be used (Valamanesh et al., 2013). The same holds if vulnerability should be studied as function of several wave parameters, such as the wave height and period (Wrang et al., 2021; Katsidoniotaki et al., 2021).

The designed fragility curve can be considered to give a conservative prediction for the availability. A WEC failure rate of 3504/year was imposed at significant wave height $H_s = 20$ m. In practice, wave energy concepts would ideally be equipped with functions that allow them to go into survivability mode during storms and harsh weather, actively reducing the expected failure rate in violent conditions. Such survivability modes have not been considered here.

Onshore wind turbines have been shown to reach availability values as high as 95%–97% of the total time (Pfaffel et al., 2017), but offshore wind turbines have a lower availability, with numbers such as 80% and 84% (Cevasco et al., 2021), although availability in the range of 90%–97% has also been reported (Wiegand and Nillesen, 2011; Garrad Hassan, 2013). The availability can be expected to reduce for OWT installed further offshore and in deeper waters (Garrad Hassan, 2013; Cevasco et al., 2021), although the published data is still scarce. The availability found in this paper is 76% and 95% for the two sites, and thus on a level comparable with offshore wind, and for the calm site also with onshore wind. The availability is significantly higher than for instance 30%, which was reported by O'Connor et al. (2012) at high resource locations. To understand these differences, it should be highlighted once more that the results are strongly dependent on the values of input parameters; higher weather thresholds and higher failure rates would reduce the availability. Göteman et al. (2018) used a similar model as the one in the present paper, but for constant instead of varying failure rates. There, it was seen that the number of available devices varied greatly with the failure and repair rates, which is to be expected. Also, high availability for wave energy systems similar to the one found in this paper have also been found in other works; for instance by Lavidas et al. (2018) where high accessibility over 90% was found in near-shore regions.

The main limitation of this paper is the lack of fullscale, measured offshore data. This data is not available due to the very limited number of offshore installations of wave energy farms. A few arrays of fullscale WECs have been installed offshore, including the Mutriku wave power plant (16 oscillating water columns installed the Basque region, Spain) (Ibarra-Berastegi et al., 2018), the Pelamis (3 attenuators installed outside Portugal), and the Uppsala University WEC (3 point-absorbers installed on the Swedish west coast) (Rahm et al., 2012); for a recent overview, see Ning and Ding (2022). Although some data have been published on the performance of these, data on the power absorption in all sea states as well as the failure rates in different wave conditions are not publicly available. Instead, our strategy has been to use the data that is available, and model the remaining required input. Future work would thus be to measure and model data that can be used as reliable input values. One important step would be to develop real fragility curves obtained from experiments and numerical simulations to obtain the meteocean-dependent failure rates. Similar to what has been done in offshore wind energy, the structural reliability could be assessed through a probabilistic reliability analysis, to determine the probability of a structure exceeding a limit state given wind and/or wave loads (Pokhrel and Seo, 2019). The output could then be used to update existing reliability databases and standards that have been developed for wave energy systems (DNV, 2005, 2008).

Research should preferably not only be accurate and reliable, but also useful for the sector. As shown in the results, availability as well as the annual delivered energy are only two measures, and it is not clear that the configuration which produces most electricity is the preferred one from a financial perspective. To identify optimal solutions, the reliability analysis should be connected to techno-economic assessments, where the technical quantities (power rating, energy delivered/not delivered, vessel operations, downtime) should be assigned economic values and the optimization should be aimed at identifying solutions with the lowest levelised cost of energy over the lifetime. The approach presented in this paper has been to evaluate varying failure rates and repair strategies in terms of net present value, cost of repair strategies, and cost of the energy not supplied. Nevertheless, it should

be remembered that financial values for wave energy are equipped with large uncertainties, as the technology is still in pre-commercial stages.

The profitability, as measured by the net present value, was shown to be maximum at both sites for WECs with low rated power. This is to be understood from the fact that both sites represent mild wave climates, with average energy flux 3.1 kW/m at the SE site and 7.9 kW/m at the US site. As a comparison, the average energy flux at the WaveHub site on the UK coast is 20 kW/m (van Nieuwkoop et al., 2013). For a wave farm installation at a more energetic site, WECs with higher rated power would become the more optimal option, which would mean that more power could be absorbed by the available devices. On the other hand, a more energetic site would present fewer and shorter open weather windows, limiting the repair and maintenance to very short periods during the year. This was confirmed by O'Connor et al. (2012, 2013b) in their assessment of some energetic sites at the Irish west coast. The aim of the current paper was to analyse the effect of weather-dependent failure rates and resilience of wave farms. Future work could apply the same methodology but for a larger set of offshore sites, in particular more energetic sites, to assess the optimal rated power and wave farm feasibility over larger offshore areas.

Another direction of future research would be to combine the metocean-dependent failure rate proposed in this paper with a “bathtub” failure rate depending on fatigue or ageing of the WECs, and study the performance of the wave farm over longer periods of time.

5. Conclusions

The vulnerability to violent ocean conditions and the related limited access for maintenance and repair operations is one of the main challenges for new offshore RES that must be addressed to reach an economic competitiveness. This paper has addressed this problem by introducing metocean dependent failure rates for a wave energy system and analysing the availability and resilience based on this.

As compared to a weather dependent failure rate, the common assumption of a constant failure rate was seen to underestimate the failure rate in energetic wave conditions, but overestimate it in calm conditions. As a result, the constant failure rate will overpredict the annual energy absorption in the park. Perhaps more importantly than the annual energy absorption, a constant failure rate will lead to misleading prediction of the actual number of available and failed devices, which is a problem when planning and conducting the costly offshore repair operations.

Two different offshore sites were compared, and the average failure rate was found to be lower at the calmer site, whereas the potential profitability as measured by the net present value was higher at the more energetic site. Small, cheap WECs led to higher profitability than larger, more expensive ones, in particular at the calmer site.

Wave park resilience and different repair vessel strategies were evaluated from economic perspectives. In some cases, the cost of the repair operations were found to exceed the cost of the energy not supplied due to failed devices.

CRedit authorship contribution statement

Malin Götteman: Conceptualization, Data curation, Formal analysis, Funding acquisition, Investigation, Methodology, Project administration, Supervision, Visualization, Writing – original draft, Writing – review & editing. **Zahra Shahroozi:** Data curation, Formal analysis, Investigation, Visualization, Writing – original draft. **Charitini Stavropoulou:** Formal analysis, Investigation, Writing – original draft. **Eirini Katsidoniotaki:** Investigation. **Jens Engström:** Investigation, Resources, Supervision, Writing – review & editing.

Declaration of competing interest

The authors declare that they have no known competing financial interests or personal relationships that could have appeared to influence the work reported in this paper.

Data availability

Data will be made available on request

Acknowledgements

The research in this paper was supported by the Centre of Natural Hazards and Disaster Science (CNDS), Sweden, and the Swedish Research Council (grant number 2020-03634).

References

- Aizpurua, J.I., Penalba, M., Kirillova, N., Lekube, J., Marina, D., 2022. Context-informed conditional anomaly detection approach for wave power plants: The case of air turbines. *Ocean Eng.* 253, 111196.
- Astariz, S., Iglesias, G., 2015. The economics of wave energy: A review. *Renew. Sustain. Energy Rev.* 45, 397–408.
- Bard, J., Thalemann, F., 2012. Offshore Infrastructure: Ports and Vessels. a Report of the Off-Shore Renewable Energy Conversion Platforms. Technical Report Grant agreement ID 241421, Off-shore renewable energy conversion platforms coordination action.
- Behrens, S., Hayward, J., Hemer, M., Osman, P., 2012. Assessing the wave energy converter potential for Australian coastal regions. *Renew. Energy* 43, 210–217.
- Bie, Z., Lin, Y., Li, G., Li, F., 2017. Battling the extreme: A study on the power system resilience. *Proc. IEEE* 105 (7), 1253–1266.
- Black, Veatch, 2012. Cost and Performance Data for Power Generation Technologies. Technical Report, NREL National Renewable Energy Laboratory.
- Cai, Y., Hames, D., 2010. Minimum sample size determination for generalized extreme value distribution. *Commun. Stat.—Simul. Comput.* 40 (1), 87–98.
- Callaghan, J., Boud, R., 2006. Future marine energy. In: Results of the Marine Energy Challenge: Cost Competitiveness and Growth of Wave and Tidal Stream Energy. Technical Report 40, Carbon trust.
- Carroll, J., McDonald, A., McMillan, D., 2016. Failure rate, repair time and unscheduled O&M cost analysis of offshore wind turbines. *Wind Energy* 19 (6), 1107–1119.
- Cevasco, D., Koukoura, S., Kolios, A., 2021. Reliability, availability, maintainability data review for the identification of trends in offshore wind energy applications. *Renew. Sustain. Energy Rev.* 136, 110414.
- Chang, G., Jones, C.A., Roberts, J.D., Neary, V.S., 2018. A comprehensive evaluation of factors affecting the levelized cost of wave energy conversion projects. *Renew. Energy* 127, 344–354.
- Chatzigiannakou, M.A., 2019. Offshore deployments of marine energy converters (Ph.D. thesis). Uppsala University, Sweden.
- Chatzigiannakou, M.A., Dolguntseva, I., Leijon, M., 2014. Offshore deployment of point absorbing wave converters with a direct driven linear generator power take-off at the Lysekil test site. In: International Conference on Offshore Mechanics and Arctic Engineering, Vol. 45530. American Society of Mechanical Engineers, V09AT09A023.
- Chozas, J.F., Kofoed, J.P., Jensen, N.E.H., 2014. User Guide—Coe Calculation Tool for Wave Energy Converters. Technical Report Version 1.6, Department of Civil Engineering, Aalborg University.
- Clark, C.E., DuPont, B., 2018. Reliability-based design optimization in offshore renewable energy systems. *Renew. Sustain. Energy Rev.* 97, 390–400.
- Clarkson, 2022. Clarkson, Norway. <https://www.clarksons.com/>.
- Coe, R.G., Yu, Y.-H., Van Rij, J., 2018. A survey of WEC reliability, survival and design practices. *Energies* 11 (1), 4.
- Contestabile, P., Di Lauro, E., Buccino, M., Vicinanza, D., 2017. Economic assessment of overtopping breakwater for energy conversion (OBREC): a case study in Western Australia. *Sustainability* 9 (1), 51.
- Cretu, A., Munteanu, R., Iudean, D., Vladareanu, V., Karaisas, P., 2016. Reliability assessment of linear generator type wave energy converters. In: 2016 International Conference on Applied and Theoretical Electricity, ICATE, IEEE, pp. 1–5.
- Dalgic, Y., Dinwoodie, I.A., Lazakis, I., McMillan, D., Revie, M., 2014. Optimum CTW fleet selection for offshore wind farm O&M activities. In: ESREL 2014.
- de Andrés, A.D., Jeffrey, H., Guanche, R., 2015. Finding locations for wave energy development as a function of reliability metrics. In: Proceedings of the 11th European Wave and Tidal Energy Conference. EWTEC, Nantes, France.
- de Andrés, A., Maillet, J., Hals Todalshaug, J., Möller, P., Bould, D., Jeffrey, H., 2016. Techno-economic related metrics for a wave energy converters feasibility assessment. *Sustainability* 8 (11), 1109.
- DNV, 2005. Guidelines on Design and Operation of Wave Energy Converters. Technical Report, Carbon Trust.
- DNV, 2008. Certification of Tidal and Wave Energy Converters. Technical Report DNV-OSS-312.
- DNV, 2011. Modelling and Analysis of Marine Operations. Recommended Practice: DNV-RP-H103.
- Dunnett, D., Wallace, J.S., 2009. Electricity generation from wave power in Canada. *Renew. Energy* 34 (1), 179–195.

- Engström, J., Göteman, M., Eriksson, M., Bergkvist, M., Nilsson, E., Rutgersson, A., Strömstedt, E., 2020. Energy absorption from parks of point-absorbing wave energy converters in the Swedish exclusive economic zone. *Energy Sci. Eng.* 8 (1), 38–49.
- Ericsson, E., Gregorson, E., 2018. Quantitative Risk Assessment of Wave Energy Technology (Master's thesis). Uppsala University, Sweden.
- Eriksson, M., Waters, R., Svensson, O., Isberg, J., Leijon, M., 2007. Wave power absorption: Experiments in open sea and simulation. *J. Appl. Phys.* 102 (8), 084910.
- Espinoza, S., Panteli, M., Mancarella, P., Rudnick, H., 2016. Multi-phase assessment and adaptation of power systems resilience to natural hazards. *Electr. Power Syst. Res.* 136, 352–361.
- Feng, Q., Zhao, X., Fan, D., Cai, B., Liu, Y., Ren, Y., 2019. Resilience design method based on meta-structure: A case study of offshore wind farm. *Reliab. Eng. Syst. Saf.* 186, 232–244.
- Fisher, R.A., Tippett, L.H.C., 1928. Limiting forms of the frequency distribution of the largest or smallest member of a sample. In: *Mathematical Proceedings of the Cambridge Philosophical Society*, Vol. 24. Cambridge University Press, pp. 180–190.
- Gallagher, S., Tiron, R., Whelan, E., Gleeson, E., Dias, F., McGrath, R., 2016. The nearshore wind and wave energy potential of Ireland: a high resolution assessment of availability and accessibility. *Renew. Energy* 88, 494–516.
- Garrad Hassan, G., 2013. A Guide to UK Offshore Wind Operations and Maintenance. Technical Report 2013:42, Scottish Enterprise.
- Giassi, M., Castellucci, V., Engström, J., Göteman, M., 2019. An economical cost function for the optimization of wave energy converter arrays. In: *The 29th International Ocean and Polar Engineering Conference*.
- Giassi, M., Castellucci, V., Göteman, M., 2020. Economical layout optimization of wave energy parks clustered in electrical subsystems. *Appl. Ocean Res.* 101, 102274.
- Gintautas, T., Sørensen, J.D., 2017. Improved methodology of weather window prediction for offshore operations based on probabilities of operation failure. *J. Mar. Sci. Eng.* 5 (2), 20.
- Gnedenko, B., 1943. Sur la distribution limite du terme maximum d'une serie aleatoire. *Ann. of Math.* 423–453.
- Göteman, M., 2022. Passive damping control in wave farms using cluster communication. *Trends Renew. Energies Offshore* 385–392.
- Göteman, M., Engström, J., Eriksson, M., Hann, M., Ransley, E., Greaves, D., Leijon, M., 2015a. Wave loads on a point-absorbing wave energy device in extreme waves. *J. Ocean Wind Energy* 2 (3), 176–181.
- Göteman, M., Engström, J., Eriksson, M., Isberg, J., 2015b. Fast modeling of large wave energy farms using interaction distance cut-off. *Energies* 8 (12), 13741–13757.
- Göteman, M., Giassi, M., Engström, J., Isberg, J., 2020. Advances and challenges in wave energy park optimization—A review. *Front. Energy Res.* 8, 26.
- Göteman, M., Mathew, J., Engström, J., Castellucci, V., Giassi, M., Waters, R., 2018. Wave energy farm performance and availability as functions of weather windows. In: *Proceedings of the 3rd International Conference on Renewable Energies Offshore*. RENEW, Lisbon, Portugal.
- Guanche, R., de Andrés, A., Losada, I., Vidal, C., 2015. A global analysis of the operation and maintenance role on the placing of wave energy farms. *Energy Convers. Manage.* 106, 440–456.
- Gueguen, S., 2016. Risk Assessment of Marine Energy Projects (Master's thesis). KTH Royal Institute of Technology, Sweden.
- Haas, K.A., Fritz, H.M., French, S.P., Smith, B.T., Neary, V., 2011. Assessment of Energy Production Potential from Tidal Streams in the United States. Technical Report, Georgia Tech Research Corporation, Atlanta, GA (United States).
- Hann, M., Greaves, D., Raby, A., 2015. Snatch loading of a single taut moored floating wave energy converter due to focussed wave groups. *Ocean Eng.* 96, 258–271.
- Hayward, J., Behrens, S., McGarry, S., Osman, P., 2012. Economic modelling of the potential of wave energy. *Renew. Energy* 48, 238–250.
- Ibarra-Berastegi, G., Sáenz, J., Ulazia, A., Serras, P., Esnaola, G., Garcia-Soto, C., 2018. Electricity production, capacity factor, and plant efficiency index at the Mutriku wave farm (2014–2016). *Ocean Eng.* 147, 20–29.
- IEC International Electrotechnical Commission, 2015. Marine Energy: Wave, Tidal and Other Water Current Converters. Tidal Energy Resource Assessment and Characterization. Technical Report IEC TS 62600-2:2016-08.
- Ingram, D.M., 2011. Protocols for the Equitable Assessment of Marine Energy Converters. Lulu. com.
- Ioannou, A., Angus, A., Brennan, F., 2018. A lifecycle techno-economic model of offshore wind energy for different entry and exit instances. *Appl. Energy* 221, 406–424.
- Jacobson, P.T., Hagerman, G., Scott, G., 2011. Mapping and Assessment of the United States Ocean Wave Energy Resource. Technical Report, Electric Power Research Institute.
- Jonathan, P., Ewans, K., 2007. Uncertainties in extreme wave height estimates for hurricane-dominated regions. *J. Offshore Mech. Arct. Eng.* 129 (4), 300–305.
- Jonathan, P., Ewans, K., 2013. Statistical modelling of extreme ocean environments for marine design: a review. *Ocean Eng.* 62, 91–109.
- Katsidoniotaki, E., Nilsson, E., Rutgersson, A., Engström, J., Göteman, M., 2021. Response of point-absorbing wave energy conversion system in 50-years return period extreme focused waves. *J. Mar. Sci. Eng.* 9 (3), 345.
- Kennedy, B., Weber, J., Nielsen, K., Hanafin, J., Costello, R., 2017. Wave farm design: Optimisation of O&M with respect to weather window criteria. In: *Proceedings of the 12th European Wave and Tidal Energy Conference*. EWTEC, Cork, Ireland.
- Kiel, E.S., Kjølle, G.H., 2019. The impact of protection system failures and weather exposure on power system reliability. In: *2019 IEEE Int. Conf. on Environment and Electrical Engineering and 2019 IEEE Industrial and Commercial Power Systems Europe*.
- Korde, U.A., 2019. Enhancing the resilience of energy systems: Optimal deployment of wave energy devices following coastal storms. *J. Renew. Sustain. Energy* 11 (3), 034501.
- Lacroix, D., Lamblin, V., Paillard, M., 2009. Marine Renewable Energies: Prospective Foresight Study for 2030. Editions Quae.
- Lavidas, G., 2019. Energy and socio-economic benefits from the development of wave energy in Greece. *Renew. Energy* 132, 1290–1300.
- Lavidas, G., Agarwal, A., Venugopal, V., 2018. Availability and accessibility for offshore operations in the Mediterranean Sea. *J. Waterw. Port Coast. Ocean Eng.* 144 (6), 05018006.
- Madhi, F., Yeung, R.W., 2018. On survivability of asymmetric wave-energy converters in extreme waves. *Renew. Energy* 119, 891–909.
- Martini, M., Guanache, R., Losada, I.J., Vidal, C., 2017. Accessibility assessment for operation and maintenance of offshore wind farms in the North Sea. *Wind Energy* 20 (4), 637–656.
- Mérigaud, A., Ringwood, J.V., 2016. Condition-based maintenance methods for marine renewable energy. *Renew. Sustain. Energy Rev.* 66, 53–78.
- van Nieuwkoop, J.C., Smith, H.C., Smith, G.H., Johanning, L., 2013. Wave resource assessment along the Cornish coast (UK) from a 23-year hindcast dataset validated against buoy measurements. *Renew. Energy* 58, 1–14.
- Ning, D., Ding, B., 2022. Modelling and Optimization of Wave Energy Converters. CRC Press.
- Noguera, C., Dhedin, J., Saviot, S., Stallard, T., 2010. Procedures for Estimating Site Accessibility and Appraisal of Implications of Site Accessibility. Technical Report, European Commission.
- O'Connor, M., Burke, D., Curtin, T., Lewis, T., Dalton, G., 2012. Weather windows analysis incorporating wave height, wave period, wind speed and tidal current with relevance to deployment and maintenance of marine renewables. In: *Proceedings of the 4th International Congress on Ocean Energy*. Dublin, Ireland.
- O'Connor, M., Lewis, T., Dalton, G., 2013a. Operational expenditure costs for wave energy projects and impacts on financial returns. *Renew. Energy* 50, 1119–1131.
- O'Connor, M., Lewis, T., Dalton, G., 2013b. Weather window analysis of Irish west coast wave data with relevance to operations & maintenance of marine renewables. *Renew. Energy* 52, 57–66.
- OES Ocean Energy Systems, 2015. International Levelised Cost of Energy for Ocean Energy Technologies. Technical Report, IEA International Energy Agency.
- Oliveira-Pinto, S., Rosa-Santos, P., Taveira-Pinto, F., 2019. Electricity supply to offshore oil and gas platforms from renewable ocean wave energy: Overview and case study analysis. *Energy Convers. Manage.* 186, 556–569.
- Panteli, M., Mancarella, P., 2015. The grid: Stronger, bigger, smarter?: Presenting a conceptual framework of power system resilience. *IEEE Power Energy Mag.* 13 (3), 58–66.
- Pascal, R., Gorintin, F., Payne, G.S., Cliquet, V., 2018. The right size for a WEC: a study on the consequences of the most basic design choice. In: *Proceedings of the 7th International Conference on Ocean Energy*. Cherbourg, France, pp. 12–14.
- Pfaffel, S., Faulstich, S., Rohrig, K., 2017. Performance and reliability of wind turbines: A review. *Energies* 10 (11), 1904.
- Pokhrel, J., Seo, J., 2019. Natural hazard vulnerability quantification of offshore wind turbine in shallow water. *Eng. Struct.* 192, 254–263.
- Rademakers, L., Braam, H., Obdam, T., Van de Pieterman, R., 2009. Energy Research Centre of the Netherlands.
- Rafiee, A., Fiévez, J., 2015. Numerical prediction of extreme loads on the CETO wave energy converter. In: *Proceedings of the 11th European Wave and Tidal Energy Conference*, Nantes, France.
- Rahm, M., Svensson, O., Boström, C., Waters, R., Leijon, M., 2012. Experimental results from the operation of aggregated wave energy converters. *IET Renew. Power Gener.* 6 (3), 149–160.
- Ransley, E.J., 2015. Survivability of Wave Energy Converter and Mooring Coupled System Using CFD (Ph.D. thesis). Plymouth University, UK.
- Rémouit, F., Chatzigiannakou, M.-A., Bender, A., Temiz, I., Sundberg, J., Engström, J., 2018. Deployment and maintenance of wave energy converters at the Lysekil research site: A comparative study on the use of divers and remotely-operated vehicles. *J. Mar. Sci. Eng.* 6 (2), 39.
- Rinaldi, G., Johanning, L., Thies, P., Walker, R., 2016a. A novel reliability-based simulation tool for offshore renewable technologies. In: *Proceedings of the 2nd International Conference on Renewable Energies*. RENEW, Lisbon, Portugal.
- Rinaldi, G., Portillo, J., Khalid, F., Henriques, J., Thies, P., Gato, L., Johanning, L., 2018. Multivariate analysis of the reliability, availability, and maintainability characterizations of a spar-buoy wave energy converter farm. *J. Ocean Eng. Mar. Energy* 4 (3), 199–215.
- Rinaldi, G., Thies, P.R., Walker, R., Johanning, L., 2016b. On the analysis of a wave energy farm with focus on maintenance operations. *J. Mar. Sci. Eng.* 4 (3), 51.
- Schwartz, M., Heimiller, D., Haymes, S., Musial, W., 2010. Assessment of Offshore Wind Energy Resources for the United States. Technical Report, National Renewable Energy Lab (NREL), Golden, CO (United States).

- Silva, N., Estanqueiro, A., 2013. Impact of weather conditions on the windows of opportunity for operation of offshore wind farms in Portugal. *Wind Eng.* 37 (3), 257–268.
- Sjökvist, L., Wu, J., Ransley, E., Engström, J., Eriksson, M., Götteman, M., 2017. Numerical models for the motion and forces of point-absorbing wave energy converters in extreme waves. *Ocean Eng.* 145, 1–14.
- Smart, G., Smith, A., Warner, E., Sperstad, I.B., Prinsen, B., Lacal-Arantegui, R., 2016. IEA Wind Task 26: Offshore Wind Farm Baseline Documentation. Technical Report, National Renewable Energy Lab (NREL), Golden, CO (United States).
- Soerensen, H., Friis-Madsen, E., 2010. Wave Dragon 1.5 MW North Sea Demonstrator Phase 1. Technical Report EUDP 2010-II 64010-0405, Wave Dragon, Final Report, Danish Energy Authority.
- Stavropoulou, C., Götteman, M., 2022. A very simple park interaction factor. In: Proc. of the 37th Intl. Workshop on Water Waves and Floating Bodies. IWWWFB, Giardini Naxos, Italy.
- Stehly, T., Beiter, P., Duffy, P., 2020. 2019 Cost of Wind Energy Review. Technical Report, National Renewable Energy Lab (NREL), Golden, CO (United States).
- Tan, J., Polinder, H., Laguna, A.J., Wellens, P., Miedema, S.A., 2021. The influence of sizing of wave energy converters on the techno-economic performance. *J. Mar. Sci. Eng.* 9 (1), 52.
- Teillant, B., Costello, R., Weber, J., Ringwood, J., 2012. Productivity and economic assessment of wave energy projects through operational simulations. *Renew. Energy* 48, 220–230.
- Têtu, A., Fernandez Chozas, J., 2021. A proposed guidance for the economic assessment of wave energy converters at early development stages. *Energies* 14 (15), 4699.
- Thies, P.R., Flinn, J., Smith, G.H., 2009. Is it a showstopper? Reliability assessment and criticality analysis for wave energy converters. Proceedings of the 8th European Wave and Tidal Energy Conference (EWTEC), Uppsala, Sweden.
- Thies, P.R., Johanning, L., Smith, G.H., 2011. Towards component reliability testing for marine energy converters. *Ocean Eng.* 38 (2–3), 360–370.
- TraidMachinery, 2022. Triad machinery. <https://tradmachinery.com/>.
- Valamanesh, V., Myers, A., Hajjar, J., Arwade, S., 2013. Probabilistic modeling of joint hurricane-induced wind and wave hazards to offshore wind farms on the Atlantic coast. In: Deodatis, G., Ellingwood, B.R., Frangopol, D.M. (Eds.), *Safety, Reliability, Risk and Life-Cycle Performance of Structures and Infrastructures*, Vol. 247. Taylor & Francis Group, London.
- Vieira, M., Snyder, B., Henriques, E., Reis, L., 2019. European offshore wind capital cost trends up to 2020. *Energy Policy* 129, 1364–1371.
- Walker, R.T., Johanning, L., Parkinson, R., 2011. Weather windows for device deployment at UK test sites: availability and cost implications. In: Proceedings of the 9th European Wave and Tidal Energy Conference. EWTEC, Southampton, UK.
- Walker, R.T., van Nieuwkoop-McCall, J., Johanning, L., Parkinson, R.J., 2013. Calculating weather windows: Application to transit, installation and the implications on deployment success. *Ocean Eng.* 68, 88–101.
- Wang, Q., Yu, Z., Ye, R., Lin, Z., Tang, Y., 2019. An ordered curtailment strategy for offshore wind power under extreme weather conditions considering the resilience of the grid. *IEEE Access* 7, 54824–54833.
- Weller, S.D., Thies, P.R., Gordelier, T., Johanning, L., 2015. Reducing reliability uncertainties for marine renewable energy. *J. Mar. Sci. Eng.* 3 (4), 1349–1361.
- Wiegand, M., Nillesen, P., 2011. Offshore Proof. Turning Windpower Promise into Performance. Technical Report, PricewaterhouseCoopers PwC, London, UK.
- Wolfram, J., 2006. On assessing the reliability and availability of marine energy converters: the problems of a new technology. *Proc. Inst. Mech. Eng. O* 220 (1), 55–68.
- Wrang, L., Katsidoniotaki, E., Nilsson, E., Rutgersson, A., Rydén, J., Götteman, M., 2021. Comparative analysis of environmental contour approaches to estimating extreme waves for offshore installations for the Baltic Sea and the North Sea. *J. Mar. Sci. Eng.* 9 (1), 96.
- Zhao, X., Hu, C., 2012. Numerical and experimental study on a 2-D floating body under extreme wave conditions. *Appl. Ocean Res.* 35, 1–13.
- Zuo, H., Bi, K., Hao, H., Xin, Y., Li, J., Li, C., 2020. Fragility analyses of offshore wind turbines subjected to aerodynamic and sea wave loadings. *Renew. Energy* 160, 1269–1282.